Voltage Dependent Differentially Grown Zinc Oxide Nanowire based Three Terminal Device for Water Quality Monitoring

Thesis submitted towards partial fulfilment of the requirements for the award of the Degree of Master of Technology in Nano Science and Technology

By

KAZI WAKAR HASAN

Registration number: 163813 of 2022-2023

Class Roll No.: 002230701009

Examination Roll No.: M4NST24009

Under the guidance of

Dr. Chandan Kumar Ghosh

School of Materials Science and Nanotechnology

Jadavpur University

Kolkata-700032

INDIA

June 2024

We hereby recommend that the thesis entitled as “Voltage Dependent Differentially Grown Zinc Oxide Nanowire based Three Terminal Device for Water Quality Monitoring”, prepared by Mr. Kazi Wakar Hasan (Class Roll No: 002230701009, Registration No: 163813 of 2022-2023, Examination Roll No: M4NST24009) under our guidance, be accepted in partial fulfilment of the requirement for the award of the Degree of Master of Technology in Nano Science and Technology from the School of Materials Science and Nano Technology of Jadavpur University.

HOD/Director

Dr. Mahua Ghosh Chaudhuri

Director,

School of Materials Science & Nanotechnology,

Jadavpur University

Thesis Advisor

Dr. Chandan Kumar Ghosh

Professor,

School of Materials Science & Nanotechnology,

Jadavpur University

Dean-FISLM,

Jadavpur University,

Kolkata-700032

ACKNOWLEDGEMENT

I would like to express my deepest gratitude to my supervisor, Dr. Chandan Kumar Ghosh, Assistant Professor, School of Materials Science and Nanotechnology, Jadavpur University, for his invaluable guidance, expertise and constant support throughout this research endeavour. His mentorship has been instrumental in shaping this thesis and my growth as a researcher.

I am immensely grateful to Dr. Sayan Dey, Assistant Professor, School of Electrical Sciences, IIT Bhubaneswar, for his continuous support and motivation throughout this journey. His insightful inputs and assistance have been invaluable in overcoming challenges and pushing the boundaries of this research.

I gratefully thank Prof Kalyan Kumar Chattopadhyay, Dr. Sourav Sarkar and Dr. Mahua Ghosh Chaudhuri for their assistance, support, recommendations and guidance. They offered a helpful and constructive learning environment, and their excitement inspired me to pursue the research topic with zeal.

I would like to acknowledge and thank all the members of the Nano Lab, including Sourav Kumar Nandi, Panchanan Sahoo, Sudip Kundu, Riddhiman Sahoo, Mandira Das, Shriya Purkait, Raushan Kabir Khan, Roshni Begum, Gourab Payra, Srijita Chakraborty, Debadrita Bhaduri, and others, for their collaborative spirit, technical assistance, and stimulating discussions that have enriched my research experience.

I am grateful to the members of the VLSI Lab, Department of Electronics and Communication Engineering, School of Electrical Sciences, IIT Bhubaneswar, including

Shreyansh Mishra, Sukanya Mahalik, Mrinmay Patra, Anuvindh R., Arijit Patra and Piyush Chankapure, for their support and guidance in various aspects of my work.

Lastly, I would like to express my deepest appreciation to my parents and elder sister for their unwavering faith, unconditional love, support and encouragement throughout my academic journey. Their belief in me has been a constant source of strength and inspiration. I am grateful to everyone mentioned above, as well as any individuals who have contributed to this research in any way, for their invaluable support, which has been instrumental in the successful completion of this thesis.

-Kazi Wakar Hasan

Dedicated to my Parents

ABSTRACT

It is necessary to detect Heavy Metal Ions due to their toxic effects on the environment and human health. Chromium(VI), Copper(II), Iron(II) and Nickel(III) ions pose serious risks when present in above par concentrations in water sources, by contaminating drinking water supplies, accumulating in ecosystems and have toxic effects on aquatic life. Development of reliable and sensitive sensing devices for their detection is crucial for effective monitoring, ensuring water safety and implementing appropriate remediation strategies. This thesis focuses on the detection and analysis of specific heavy metal ions, namely Chromium(VI), Copper(II), Iron(II) and Nickel(III) ions in water samples. The material of choice for this study is Zinc Oxide, which exhibits favourable properties for sensing applications. The Zinc Oxide Nanowire based Three Terminal Devices are prepared under different Bias Voltages and their further characterization and heavy metal ion sensing is done. The synthesized materials were characterized using X-Ray Diffraction (XRD), Field Emission Scanning Electron Microscopy (FESEM) and Diffuse Reflectance Spectroscopy (DRS). The results of the sensing experiments demonstrated that the Zinc Oxide-based Three Terminal Device has better response towards Chromium(VI), Copper(II), Nickel(III) ions but not towards Iron(II) ions.

TABLE OF CONTENTS

List of Figures……1

List of Tables……...6

Chapter 1

1. Introduction……7

1.1 Preamble……7

1.2 Sensors……7

1.3 Water Quality Monitoring……9

1.4 Heavy Metal Ion Sensor……..9

1.5 Sensor Parameters……..10

1.6 Motivation for the work……11

References……12

Chapter 2

2. Literature Review……15

2.1 Introduction to Heavy Metals……15

2.2 Sources of Heavy Metal Ions……15

2.2.1 Chromium (Cr)…….....16

2.2.2 Copper (Cu)……...17

2.2.3 Iron (Fe)…….17

2.2.4 Nickel (Ni)…….18

2.3 Conventional Methods of Heavy Metal Ion Detection…….19

2.3.1 Atomic Absorption Spectroscopy (AAS)……..20

2.3.2 Inductively Coupled Plasma Spectroscopy (ICP)……20

2.3.3 LASER-Induced Breakdown Spectroscopy (LIBS)…….20

2.3.4 X-Ray Fluorescence (XRF)……..20

2.3.5 Neutron Activation Analysis (NAA)……21

2.3.6 Ion Chromatography (IC)…….21

2.4 Types of Heavy Metal Ion Sensors……..21

2.4.1 Optical Sensors……21

2.4.2 Electrochemical Sensors……..22

2.4.3 Semiconductor-based Heavy Metal Ion Sensor……...22

2.4.3.1 Metal Oxide Semiconductors…….....22

2.4.3.2 Transition Metal Dichalcogenides (TMDCs)……23

2.5 Fabrication of sensing layer…….24

2.5.1 Top-Down Approaches……24

2.5.2 Bottom-Up Approaches…….....25

References…….26

Chapter 3

3. Fabrication of Gated Voltage Assisted Zinc Oxide Nanowire-based n-n^+ Heterostructure Device……..31

3.1 Synthesis of Sensing Material…….31

3.1.1 Chemicals and Instruments……..31

3.1.2 Synthesis Procedure……..32

3.1.3 Variation in Synthesis Procedure……..37

3.1.4 FESEM Images observed in those variation…….37

3.1.5. X-Ray Diffraction (XRD) Analysis…….38

3.1.6 Diffuse Reflectance Spectroscopy (DRS) Data observed in those variations……45

3.2 Experimental Setup for Gated Voltage Assisted Zinc Oxide Nanowire-based n-n^+ Heterostructure……..46

3.2.1 Current(I)-Voltage(V) Characteristics observed in Bare Device……47

References…….57

Chapter 4

4. Heavy Metal Ion Sensing by Gated Voltage Assisted Zinc Oxide Nanowire-based n-n^+ Heterostructure Device……59

4.1 Results and Discussions……60

4.1.1 Sensing using Three Terminal ZnO NW-based Device under 2.5V Bias Voltage……60

4.1.2 Sensing using Three Terminal ZnO NW-based Device under 5V Bias Voltage……64

4.1.3 Sensing using Three Terminal ZnO NW-based Device under 7.5V Bias Voltage……69

4.1.4 Sensing using Three Terminal ZnO NW-based Device under 10V Bias Voltage…….73

4.1.5 Mechanism of Heavy Metal Ion Sensing……78

4.2 Overall Response of the Devices and their Selectivity……..78

Chapter 5

5. Conclusion and Future Work…….80

5.1 Conclusion……..80

5.2 Future Works……...81

LIST OF FIGURES

Figure 3.1(a): Zinc Nitrate Hexahydrate

Figure 3.1(b): Hexamethylenetetramine (HMTA)

Figure 3.1(c): 25% Ammonia Solution

Figure 3.2(a): Magnetic Stirrer with Hot Plate

Figure 3.2(b): Regulated DC Power Supply

Figure 3.3: Silver Paste deposited p-Si (100) substrate

Figure 3.4: Schematic Diagram of the Device submerged in the precursor solution

Figure 3.5: Flow Diagram for the Nucleation of ZnO Seed Layer

Figure 3.6: Flow Diagram for the Synthesis of ZnO Nanowire

Figure 3.7: Experimental Setup for the growth of ZnO Nanowire

Figure 3.8: FESEM Images of ZnO Nanowire based n-n^+ heterostructure devices (Less n-type Region in the left side & More n-type Region in the right side)

Figure 3.9(a): XRD Spectrum of Less n-type Region in ZnO Nanowire under 2.5V Bias Voltage

Figure 3.9(b): XRD Spectrum of More n-type Region in ZnO Nanowire under 2.5V Bias Voltage

Figure 3.9(c): XRD Spectrum of Less n-type Region in ZnO Nanowire under 5V Bias Voltage

Figure 3.9(d): XRD Spectrum of More n-type Region in ZnO Nanowire under 5V Bias Voltage

Figure 3.9(e): XRD Spectrum of Less n-type Region in ZnO Nanowire under 7.5V Bias Voltage

Figure 3.9(f): XRD Spectrum of More n-type Region in ZnO Nanowire under 7.5V Bias Voltage

Figure 3.9(g): XRD Spectrum of Less n-type Region in ZnO Nanowire under 10V Bias Voltage

Figure 3.9(h): XRD Spectrum of Less n-type Region in ZnO Nanowire under 10V Bias Voltage

Figure 3.10: Variation in Diffraction Peak intensities in different regions for ZnO NW under 7.5V Bias Voltage

Figure 3.11: Probe Station used for Experiment

Figure 3.12: Three Terminal arrangement in the device inside the Probe Station

Figure 3.13: Entire Experimental Setup for finding the I-V Characteristics of the Three-Terminal Device

Figure 3.14(a): IV Characteristics of Two Terminal ZnO NW-based Device under 2.5V Bias Voltage

Figure 3.14(b): IV Characteristics of Two Terminal ZnO NW-based Device under 5V Bias Voltage

Figure 3.14(c): IV Characteristics of Two Terminal ZnO NW-based Device under 7.5V Bias Voltage

Figure 3.14(d): IV Characteristics of Two Terminal ZnO NW-based Device under 10V Bias Voltage

Figure 3.15: Probable Energy Band Diagram observed in Two Terminal ZnO NW-based Device

Figure 3.16(a): I_d vs V_{ds} Curve for Three Terminal ZnO NW-based Device under 2.5V Bias Voltage (under ambient condition)

Figure 3.16(b): I_d vs V_{ds} Curve for Three Terminal ZnO NW-based Device under 5V Bias Voltage (under ambient condition)

Figure 3.16(c): I_d vs V_{ds} Curve for Three Terminal ZnO NW-based Device under 7.5V Bias Voltage (under ambient condition)

Figure 3.16(d): I_d vs V_{ds} Curve for Three Terminal ZnO NW-based Device under 10V Bias Voltage (under ambient condition)

Figure 3.17(a): Schematic Diagram of the Device under positive Gate-to-Source Voltage (V_{gs})

Figure 3.17(b): Schematic Diagram of the Device under negative Gate-to-Source Voltage (V_{gs})

Figure 4.1: Different Heavy Metal Ions used for sensing purpose

Figure 4.2(a): I_d vs V_{ds} Curve for Three Terminal ZnO NW-based Device under 2.5V Bias Voltage [exposed to 100ppm Cr(VI)]

Figure 4.2(b): I_d vs V_{ds} Curve for Three Terminal ZnO NW-based Device under 2.5V Bias Voltage [exposed to 100ppm Cu(II)]

Figure 4.2(c): I_d vs V_{ds} Curve for Three Terminal ZnO NW-based Device under 2.5V Bias Voltage [exposed to 100ppm Fe(II)]

Figure 4.2(d): I_d vs V_{ds} Curve for Three Terminal ZnO NW-based Device under 2.5V Bias Voltage [exposed to 100ppm Ni(III)]

Figure 4.3: Response vs Analyte Curves of Three Terminal ZnO NW-based Device under 2.5V Bias Voltage [V_{gs} varies from (-5)V to (+5)V]

Figure 4.4(a): I_d vs V_{ds} Curve for Three Terminal ZnO NW-based Device under 5V Bias Voltage [exposed to 100ppm Cr(VI)]

Figure 4.4(b): I_d vs V_{ds} Curve for Three Terminal ZnO NW-based Device under 5V Bias Voltage [exposed to 100ppm Cu(II)]

Figure 4.4(c): I_d vs V_{ds} Curve for Three Terminal ZnO NW-based Device under 5V Bias Voltage [exposed to 100ppm Fe(II)]

Figure 4.4(d): I_d vs V_{ds} Curve for Three Terminal ZnO NW-based Device under 5V Bias Voltage [exposed to 100ppm Ni(III)]

Figure 4.5: Response vs Analyte Curves of Three Terminal ZnO NW-based Device under 5V Bias Voltage [V_{gs} varies from (-5)V to (+5)V]

Figure 4.6(a): I_d vs V_{ds} Curve for Three Terminal ZnO NW-based Device under 7.5V Bias Voltage [exposed to 100ppm Cr(VI)]

Figure 4.6(b): I_d vs V_{ds} Curve for Three Terminal ZnO NW-based Device under 7.5V Bias Voltage [exposed to 100ppm Cu(II)]

Figure 4.6(c): I_d vs V_{ds} Curve for Three Terminal ZnO NW-based Device under 7.5V Bias Voltage [exposed to 100ppm Fe(II)]

Figure 4.6(d): I_d vs V_{ds} Curve for Three Terminal ZnO NW-based Device under 7.5V Bias Voltage [exposed to 100ppm Ni(III)]

Figure 4.7: Response vs Analyte Curves of Three Terminal ZnO NW-based Device under 7.5V Bias Voltage [V_{gs} varies from (-5)V to (+5)V]

Figure 4.8(a): I_d vs V_{ds} Curve for Three Terminal ZnO NW-based Device under 10V Bias Voltage [exposed to 100ppm Cr(VI)]

Figure 4.8(b): I_d vs V_{ds} Curve for Three Terminal ZnO NW-based Device under 10V Bias Voltage [exposed to 100ppm Cu(II)]

Figure 4.8(c): I_d vs V_{ds} Curve for Three Terminal ZnO NW-based Device under 10V Bias Voltage [exposed to 100ppm Fe(II)]

Figure 4.8(d): I_d vs V_{ds} Curve for Three Terminal ZnO NW-based Device under 10V Bias Voltage [exposed to 100ppm Ni(III)]

Figure 4.9: Response vs Analyte Curves of Three Terminal ZnO NW-based Device under 10V Bias Voltage [V_{gs} varies from (-5)V to (+5)V]

Figure 4.10: Overall Response Curves of the as-prepared Devices

LIST OF TABLES

Table 3.1: Intensities of Diffraction Peaks for Different Planes in all the devices

Table 3.2: Comparison of Particle Size from Scherrer Formula and from Williamson-Hall Plot

Table 3.3: Band Gap Energy in different regions of the devices

Table 4.1: Response of Three Terminal ZnO NW-based Device under 2.5V Bias Voltage

Table 4.2: Response of Three Terminal ZnO NW-based Device under 5V Bias Voltage

Table 4.3: Response of Three Terminal ZnO NW-based Device under 7.5V Bias Voltage

Table 4.4: Response of Three Terminal ZnO NW-based Device under 10V Bias Voltage

CHAPTER 1

1 Introduction

This chapter provides a thorough introduction to sensors, and the specific focus is on the Heavy Metal Ion Sensors. Different parameters which are used to evaluate sensors are discussed here. The motivation for present work is included. The material used to fabricate the device is described here, along with its structure and properties.

1.1 Preamble

With time human race is evolved and broaden its technological arms towards some charismatic inventions. Developing Sensors is one of the exceptional inventions. In the expansive domain of engineering, the innovation of cutting-edge sensors stands as a cornerstone in advancing our comprehension of the chemical realm, crucially addressing urgent environmental and health challenges; notably, heavy metal ions emerge as formidable foes, characterized by their pernicious toxicity, enduring presence, and alarming propensity to amass within diverse ecosystems.

This thesis immerses itself in the domain of heavy metal ion sensing, aiming to contribute to the ever-growing body of knowledge and advancements in this crucial field.Utilizing state-of-the-art methodologies and harnessing the intrinsic characteristics of heavy metal ions, this study strives to pioneer the creation of a high-performance sensor, adept at discerning and measuring these perilous elements with unparalleled precision and sensitivity.

1.2 Sensors

A Sensor is a device capable of detecting changes in physical quantities. The term "Sensor" originated from the latin word "Sentire" which means "to feel". A Sensor is a device or component that detects changes in its environment and responds by generating an output. It converts physical phenomena (such as light, temperature, pressure, or motion) into electrical signals or other readable forms. Sensors are widely used in various fields, including

automotive, consumer electronics, industrial automation, healthcare and environmental monitoring. They play a crucial role in enabling machines to perceive and interact with the world around them, facilitating automation, control and data collection processes.

In our normal life we use different types of Sensors that are commonly used in various applications. All these Sensors are used for measuring one of the physical properties like Temperature, Resistance, Capacitance, Conductance, Heat Transfer etc. We have seen different types of Sensors along with their practical applications. There are a few types of Sensors such as-

- Temperature Sensors
- InfraRed Sensors
- Proximity Sensors
- Pressure Sensors
- Level Sensors
- Smoke & Gas Sensors
- Ultrasonic Sensors
- Touch Sensors

Based on their sensing techniques and output characteristics Sensors can be categorized into the following types-

- Chemiresistive Sensors
- Conductometric Sensors
- Capacitive Sensors
- Optical Sensors
- Piezoresistive Sensors
- Colorimetric Sensors
- Electrochemical Sensors

1.3 Water Quality Monitoring

Water Quality Monitoring is crucial for several reasons:

- **Public Health**: Monitoring water quality ensures that drinking water meets safety standards, protecting public health from waterborne diseases and contaminants. Contaminated water can lead to outbreaks of illnesses such as cholera, dysentery and gastrointestinal infections.
- **Environmental Protection**: Monitoring helps safeguard aquatic ecosystems and biodiversity by identifying pollution sources and assessing the impact of human activities on water bodies. It enables the detection of pollutants like heavy metals, pesticides and nutrients that can harm aquatic life and disrupt ecosystems.
- **Resource Management**: Effective water quality monitoring supports the sustainable management of water resources by providing data for decision-making. It helps in allocating water resources efficiently, preventing overexploitation and ensuring adequate supplies for various purposes, including agriculture, industry and recreation.
- **Early Warning Systems**: Continuous monitoring allows for the early detection of water quality problems, such as contamination events or algal blooms. Early warning systems enable rapid response measures to mitigate risks and protect both human health and ecosystems.

1.4 Heavy Metal Ion Sensor

A Heavy Metal Ion Sensor serves as a vital chemical sentinel, meticulously detecting the presence of heavy metal ions within drinking water, thereby safeguarding public health and ensuring adherence to stringent safety standards. Monitoring and removing heavy metals such as Cd(II), Hg(II), Cr(VI), As(V), Cr(III), Cu(II) and Bi(III) is crucial as they tend to accumulate in the food chain and can enter living systems through food and drinkable water[1]. Heavy Metal Ion Sensors are available in diverse forms, ranging from optical, electrochemical, to semiconducting materials-based sensors, each engineered to meticulously discern the presence of heavy metal ions [2-5]. While optical methods offer precise measurements, their adoption is hindered by their high cost, dependence on skilled professionals for operation, and cumbersome nature, thereby constraining their practical application in everyday settings [6]. Electrochemical sensors, on the other hand, utilize liquid

electrolytes, which make them unsuitable for routine heavy metal ion detection by the general public.

1.5 Sensor Parameters

The sensing parameters which describe the efficiency of a chemical sensor are as follows-

- *Sensitivity:* This refers to the ability of the sensor to detect small changes in the concentration of the target analyte. High sensitivity allows for the detection of low concentrations of the analyte.
- *Selectivity:* Selectivity is the ability of the sensor to distinguish the target analyte from other substances present in the environment or sample matrix. A selective sensor responds only to the target analyte without interference from other compounds.
- *Response Time:* Response Time indicates how quickly the sensor can detect changes in analyte concentration and provide a measurable response. Faster response times are often desirable for real-time monitoring applications.
- *Detection Limit:* The detection limit is the lowest concentration of the analyte that can be reliably detected by the sensor. Lower detection limits enable the sensor to detect trace amounts of the analyte.
- *Stability:* Stability refers to the ability of the sensor to maintain its performance characteristics over time and under varying environmental conditions. A stable sensor provides consistent and reliable measurements over its operational lifespan.
- *Repeatability and Reproducibility:* Repeatability assesses the variation in sensor response when measuring the same sample multiple times under identical conditions, while reproducibility evaluates the consistency of sensor response across different instruments or testing environments.
- *Operating Range:* The operating range specifies the range of analyte concentrations over which the sensor can provide accurate and reliable measurements.

1.6 Motivation for the work

Detection and monitoring of heavy metal ions in various environmental matrices, particularly drinkable water, have become critical due to their adverse impact on human health and the ecosystem. Developing efficient and reliable sensors for the selective detection of these ions has become an urgent research priority [7-11]. In this context, the use of semiconducting materials as sensing elements presents a promising avenue for heavy metal ion sensing. Semiconductors offer unique properties that can be tailored to selectively interact with specific target ions, providing a basis for sensitive and specific detection. Metal oxide semiconductors, in particular, have demonstrated potential for heavy metal ion sensing due to their tunable properties, stability, and compatibility with sensor fabrication processes [12-17].

Motivated by the need for accurate and selective heavy metal ion sensing, this work focuses on the development of a novel sensor using a pure metal oxide semiconductor as the sensing material. By harnessing the unique properties of these semiconducting materials, we aim to design a sensor capable of effectively detecting and quantifying different heavy metal ions in complex samples, such as drinkable water. The motivation behind this research stems from the urgent demand for cost-effective, robust, and portable heavy metal ion sensors. Current detection methods often rely on expensive and complex instrumentation, limiting their accessibility and practicality. This research aims to contribute to the protection of public health and the preservation of ecosystems.

REFERENCES:

1. M. Li, H. Gou, I. Al-Ogaidi, and N. Wu, "Nanostructured sensors for detection of heavy metals: a review," ed: ACS Publications, 2013.
2. A. Nigam, N. Sharma, S. Tripathy, and M. Kumar, "Development of semiconductor based heavy metal ion sensors for water analysis: A review," Sensors and Actuators A: Physical, vol. 330, p. 112879, 2021.
3. X. Xu, S. Yang, Y. Wang, and K. Qian, "Nanomaterial-based sensors and strategies for heavy metal ion detection," Green Analytical Chemistry, vol. 2, p. 100020, 2022.
4. A. G.-M. Ferrari, P. Carrington, S. J. Rowley-Neale, and C. E. Banks, "Recent advances in portable heavy metal electrochemical sensing platforms," Environmental Science: Water Research & Technology, vol. 6, no. 10, pp. 2676-2690, 2020.
5. U. O. Aigbe et al., "Electrochemical Detection of Heavy Metals," Modified Nanomaterials for Environmental Applications: Electrochemical Synthesis, Characterization, and Properties, pp. 25-63, 2022.
6. M. E. Mahmoud, I. Kenawy, M. A. Hafez, and R. Lashein, "Removal, preconcentration and determination of trace heavy metal ions in water samples by AAS via chemically modified silica gel N-(1-carboxy-6-hydroxy) benzylidenepropylamine ion exchanger," Desalination, vol. 250, no. 1, pp. 62-70, 2010.
7. M. R. Awual, M. Ismael, M. A. Khaleque, and T. Yaita, "Ultra-trace copper (II) detection and removal from wastewater using novel meso-adsorbent," Journal of Industrial and Engineering Chemistry, vol. 20, no. 4, pp. 2332-2340, 2014.

8. B. R. Stern, "Essentiality and toxicity in copper health risk assessment: overview, update and regulatory considerations," Journal of Toxicology and Environmental Health, Part A, vol. 73, no. 2-3, pp. 114-127, 2010.
9. R. Somphonsane, T. Chiawchan, W. Bootsa-ard, and H. Ramamoorthy, "CVD Synthesis of MoS2 Using a Direct MoO2 Precursor: A Study on the Effects of Growth Temperature on Precursor Diffusion and Morphology Evolutions," Materials, vol. 16, no. 13, p. 4817, 2023.
10. M. Legrand et al., "Alpine-ice record of bismuth pollution implies a major role of military use during World War II," Scientific Reports, vol. 13, no. 1, p. 1166, 2023.
11. R. Wang, H. Li, and H. Sun, "Bismuth: environmental pollution and health effects," Encyclopedia of environmental health, p. 415, 2019.
12. Y. Deng and Y. Deng, Sensing mechanism and evaluation criteria of semiconducting metal oxides gas sensors. Springer, 2019.
13. S. Dey, S. Santra, S. K. Ray, and P. K. Guha, "Fe x Ni (1-x) O/NiO Heterojunction Based Selective VOC Sensor Device by Using Temperature Tunability," IEEE Sensors Journal, vol. 20, no. 14, pp. 7503-7508, 2019.
14. S. Dey, S. Nag, S. Santra, S. K. Ray, and P. K. Guha, "Voltage-controlled NiO/ZnO p–n heterojunction diode: A new approach towards selective VOC sensing," Microsystems & nanoengineering, vol. 6, no. 1, p. 35, 2020.
15. S. Dey, S. Santra, A. Midya, P. K. Guha, and S. K. Ray, "Synthesis of CuxNi(1− x) O coral-like nanostructures and their application in the design of a reusable toxic heavy metal ion sensor based on an adsorption-mediated electrochemical technique," Environmental Science: Nano, vol. 4, no. 1, pp. 191-202, 2017.

16. I. Singh, S. Dey, S. Santra, K. Landfester, R. Muñoz-Espí, and A. Chandra, "Cerium doped copper (II) oxide hollow nanostructures as efficient and tunable sensors for volatile organic compounds," ACS omega, vol. 3, no. 5, pp. 5029-5037, 2018.
17. S. Dey, S. Santra, S. Sen, D. Burman, S. K. Ray, and P. K. Guha, "Photon-assisted ultra-selective formaldehyde sensing by defect induced NiO-based resistive sensor," IEEE Sensors Journal, vol. 18, no. 14, pp. 5656-5661, 2018.

CHAPTER 2

2 Literature Review

This chapter deals with the introduction of Heavy Metal Ions, along with their sources and toxicity. The conventional methods for their detection and the types of different Heavy Metal Ion Sensors are also included.

2.1 Introduction to Heavy Metals

The term “Heavy Metal” was appeared in 1817 when a German Chemist named Leopold Gmelin classified the elements into Nonmetals, Light metals and Heavy Metals [1] . Heavy Metals have comparatively high densities, atomic weights and atomic numbers [2] . The densities of the Heavy Metals ranges from 3.5 g/cm^3 to above 7 g/cm^3 [3]. A little amount of Heavy Metals are necessary for metabolism in human body [4]. Chromium (Cr), Copper (Cu), Cobalt (Co), Iron (Fe), Magnesium (Mg), Manganese (Mn), Molybdenum (Mo), Nickel (Ni) and Zinc (Zn) are some of the important Heavy Metals [5,6].

2.2 Sources of Heavy Metal Ions

In recent years, there has been a mounting global public health concern stemming from the environmental degradation caused by heavy metals, exacerbated by a substantial surge in human exposure resulting from their pervasive integration across various industrial, agricultural, domestic, and technological sectors. Reported sources of heavy metals in the environment encompass geogenic, industrial, agricultural, pharmaceutical, domestic, and atmospheric effluents, with notable environmental pollution stemming from point source activities like mining and smelting operations [7,8].

Due to their toxic, carcinogenic, and non-biodegradable properties, heavy metal ions pose a significant environmental health risk, readily accumulating in ecosystems through the food chain and exerting detrimental effects on human health upon entry into the body, where they form complexes with proteins, disrupting cellular functions and potentially leading to

toxicity, organ failure, and cancer [9]. The comprehensive analysis of the environmental occurrence, resources, potential human exposure and global ramifications associated with highly toxic heavy metal ions such as Chromium (Cr), Copper (Cu), Iron (Fe), Nickel (Ni) are described as follows.

2.2.1 Chromium (Cr)

Chromium (Cr) is a heavy metal that can pose significant health risks to humans, primarily depending on its oxidation state: hexavalent chromium (Cr(VI)) and trivalent chromium (Cr(III)). Here are some potential health risks associated with chromium exposure:

Hexavalent Chromium (Cr(VI)): This form of chromium is considered more toxic and carcinogenic than trivalent chromium.

- Cancer: Prolonged exposure to hexavalent chromium, particularly through inhalation, has been linked to lung cancer, as well as cancers of the nasal cavity and sinuses.
- Respiratory Issues: Inhalation of hexavalent chromium can cause respiratory problems such as asthma, bronchitis, and irritation of the nose, throat and lungs.
- Skin Irritation: Contact with hexavalent chromium compounds can lead to skin irritation, dermatitis and allergic reactions.

Trivalent Chromium (Cr(III)): While generally considered less toxic than hexavalent chromium, high levels of exposure to trivalent chromium can still pose health risks.

- Kidney Damage: Chronic exposure to high levels of trivalent chromium may lead to kidney damage and renal failure.
- Allergic Reactions: Some individuals may develop allergic reactions to trivalent chromium, leading to dermatitis or eczema.
- Gastrointestinal Issues: Ingestion of high doses of trivalent chromium can cause gastrointestinal irritation, nausea, vomiting and diarrhea.

2.2.2 Copper (Cu)

Copper (Cu) is an essential micronutrient for humans, but excessive exposure to copper, particularly in its metallic or inorganic forms, can lead to health risks. Here are some potential health risks associated with copper exposure:

- Gastrointestinal Issues: Ingestion of large amounts of copper can cause gastrointestinal symptoms such as nausea, vomiting, abdominal pain and diarrhea. This typically occurs when people ingest contaminated food or water.
- Liver Damage: Chronic exposure to high levels of copper can lead to liver damage and dysfunction. This is particularly relevant in cases of copper overload disorders such as Wilson's disease, where the body is unable to properly metabolize and excrete copper, leading to its accumulation in the liver and other organs.
- Neurological Effects: Excessive copper levels have been associated with neurological symptoms such as headache, dizziness and even neurological disorders like Parkinson's disease.
- Hemolytic Anemia: In rare cases, high levels of copper can cause hemolytic anemia, a condition where red blood cells are destroyed faster than they can be produced, leading to fatigue, weakness and other symptoms associated with anemia.
- Kidney Damage: Prolonged exposure to elevated copper levels may also affect kidney function, potentially leading to kidney damage or failure.
- Skin Irritation: Direct contact with copper or copper-containing compounds can cause skin irritation, allergic reactions, and dermatitis in sensitive individuals.

2.2.3 Iron (Fe)

Iron (Fe) is an essential mineral for human health, playing a crucial role in various physiological processes such as oxygen transport, energy production and DNA synthesis. However, excessive iron intake or exposure can lead to health risks, particularly in vulnerable populations. Here are some potential health risks associated with iron:

- Iron Overload: Hemochromatosis is a genetic disorder characterized by excessive absorption and accumulation of iron in the body. This can lead to iron overload, which

may cause damage to organs such as the liver, pancreas, heart and joints. Symptoms of iron overload can include fatigue, joint pain, abdominal pain and liver dysfunction.

- Gastrointestinal Distress: Acute ingestion of large amounts of iron supplements or iron-containing products can cause gastrointestinal distress, including nausea, vomiting, abdominal pain, and diarrhea. In severe cases, it can lead to gastrointestinal bleeding and damage to the lining of the digestive tract.
- Hemochromatosis-related Complications: Individuals with hemochromatosis are at an increased risk of developing complications such as liver cirrhosis, diabetes, heart disease and certain types of cancer (e.g., liver cancer).
- Iron Toxicity in Children: Accidental ingestion of iron supplements by children can be particularly dangerous and potentially fatal. Iron poisoning in children can lead to symptoms such as vomiting, diarrhea, abdominal pain, lethargy and in severe cases, organ failure and death.
- Interference with Nutrient Absorption: Excessive iron intake can interfere with the absorption of other essential nutrients such as zinc and copper. This can lead to deficiencies in these nutrients, which are also important for various physiological functions.
- Oxidative Stress: Iron can contribute to oxidative stress in the body by promoting the production of reactive oxygen species (ROS). Prolonged oxidative stress can damage cells and tissues and contribute to the development of chronic diseases such as cardiovascular disease, cancer, and neurodegenerative disorders.

2.2.4 Nickel (Ni)

Nickel (Ni) is a metallic element that is widely used in various industrial processes and consumer products. Exposure to nickel can occur through inhalation, ingestion or skin contact and prolonged or excessive exposure can lead to various health risks. Here are some potential health risks associated with nickel exposure:

- Allergic Contact Dermatitis: Nickel is one of the most common causes of allergic contact dermatitis, a skin condition characterized by redness, itching, swelling and blistering of the skin upon contact with nickel-containing materials such as jewellery,

clothing fasteners and metal tools. This allergic reaction can occur even with very small amounts of nickel exposure and may affect individuals of all ages.

- Respiratory Effects: Inhalation of nickel-containing dust or fumes, particularly in occupational settings such as nickel refining, welding and electroplating, can irritate the respiratory tract and lead to symptoms such as coughing, wheezing, shortness of breath and nasal congestion. Prolonged exposure to high levels of airborne nickel may also increase the risk of respiratory conditions such as asthma and chronic bronchitis.
- Carcinogenicity: Some forms of nickel compounds, particularly compounds containing nickel(II) oxide, have been classified as human carcinogens by organizations such as the International Agency for Research on Cancer (IARC). Occupational exposure to these carcinogenic forms of nickel has been associated with an increased risk of lung cancer and nasal cancer, particularly among workers in nickel refining, alloy production and nickel plating industries.
- Gastrointestinal Effects: Ingestion of soluble forms of nickel, such as nickel sulphate, can cause gastrointestinal irritation, nausea, vomiting, abdominal pain and diarrhea. Accidental ingestion of nickel-containing substances, such as contaminated food or water, can lead to acute toxicity, although severe cases are rare.
- Immunological Effects: Nickel exposure has been implicated in immune system dysfunction and hypersensitivity reactions, including autoimmune disorders and immune-mediated diseases.
- Cardiovascular Effects: Emerging research suggests that chronic exposure to nickel may be associated with adverse effects on cardiovascular health, including increased risk of hypertension, atherosclerosis and cardiovascular mortality.

2.3 Conventional Methods of Heavy Metal Ion Detection

Conventional analysis of heavy metals entails the utilization of standard spectroscopic methodologies, including Atomic Absorption Spectroscopy (AAS), Inductively Coupled Plasma spectrometry (ICP), Laser-Induced Breakdown Spectroscopy (LIBS), X-ray Fluorescence (XRF), Neutron Activation Analysis (NAA), and Ion Chromatography (IC).

2.3.1 Atomic Absorption Spectroscopy (AAS)

Atomic Absorption Spectroscopy (AAS) stands as a widely adopted method for trace analysis of heavy metal ions across diverse sample types, allowing for the singular determination of each element [10]. Furthermore, both cold vapor-atomic fluorescence spectroscopy (CV-AFS) and cold vapor AAS (CV-AAS) find application in analogous endeavours.

2.3.2 Inductively Coupled Plasma Spectroscopy (ICP)

Inductively Coupled Plasma Spectrometry (ICP) serves as a versatile methodology for the simultaneous analysis of multiple elements, distinguished into two main approaches: Inductively Coupled Plasma-Optical Emission Spectroscopy (ICP-OES) and Inductively Coupled Plasma-Mass Spectrometry (ICP-MS) [11,12].

2.3.3 LASER-Induced Breakdown Spectroscopy (LIBS)

LASER-Induced Breakdown Spectroscopy (LIBS) emerges as a versatile and dynamic method, facilitating swift analysis and monitoring of heavy metals in water, leveraging their distinct spectral signatures for elemental identification. LIBS stands out for its rapid, non-destructive approach, rendering it invaluable for a myriad of applications including environmental surveillance, industrial quality assurance and scientific inquiry [13].

2.3.4 X-Ray Fluorescence (XRF)

X-Ray Fluorescence (XRF) stands as a pivotal method for scrutinizing the elemental constitution of samples, harnessing X-Ray tubes to generate primary excitation sources that provoke the emission of distinctive X-Ray photons from the sample's constituent elements; subsequently, these emitted photons are meticulously detected and scrutinized through specialized detectors, enabling precise identification and quantification of the sample's elemental components grounded on their characteristic X-Ray emissions [14,15].

2.3.5 Neutron Activation Analysis (NAA)

Neutron Activation Analysis (NAA) emerges as an extraordinarily sensitive technique for quantifying the concentrations of diverse heavy metals, synergizing the precision of neutron irradiation with the scrutiny of emitted radiation from the radioactive specimen; through meticulous examination of the emitted radiation spectra, it facilitates precise determination of various elemental concentrations, proving particularly invaluable in discerning trace quantities of heavy metals in samples owing to its exceptional sensitivity [16].

2.3.6 Ion Chromatography (IC)

Ion Chromatography (IC), a streamlined approach, facilitates concurrent analysis and precise quantification of heavy metal ions in solution, harnessing High-Performance Liquid Chromatography (HPLC) principles and ion exchange resins to discern multiple ionic species in aqueous solutions, achieving detection even at parts per million (ppm) and parts per billion (ppb) levels; distinguished by its superiority in cation analysis compared to spectroscopic methods, Ion Chromatography proves especially beneficial in meticulously detecting and measuring heavy metal ions across diverse environmental, industrial, and biological samples [17].

2.4 Types of Heavy Metal Ion Sensors

2.4.1 Optical Sensors

The optical behaviour of spherical gold nanoparticles (Au NPs), characterized by a singular absorption band stemming from the collective dipole oscillation known as Surface Plasmon Resonance (SPR), underscores their utility in sensors leveraging this phenomenon, with Au NPs' tunable optical and electronic properties allowing for varied sensor applications; ranging from ruby red for smaller particles to purple or deep blue for larger particles or aggregates, the colour of Au NPs signifies their size. In sensor functionality, the introduction of specific analytes may induce uncontrolled aggregation of Au NPs via binding,

prompting a discernible change in solution colour indicative of Surface Plasmon Resonance alteration, attributed to subtle modifications in the surrounding medium's refractive index or alterations in NP interactions during analyte binding. Fluorescent sensors based on two-dimensional nanomaterials, such as graphene nanosheets, have gained significant attention for the detection of heavy metal ions [18,19].

2.4.2 Electrochemical Sensors

Nanomaterial-based electrochemical sensors, widely utilized for swift heavy metal ion detection, synergistically enhance the functionalities of optical sensors, leveraging the electrocatalytic properties of the working electrode within a redox system to discern analytes, with selectivity governed by oxidation peak positioning and sensitivity gauged by reaction current; the efficacy of these sensors crucially hinges on the selection of electrode materials. Nanomaterials have emerged as prime candidates for electrode materials in electrochemical sensors, owing to their diminutive size, expansive surface area, and potent catalytic prowess, with a diverse array of nanomaterials such as nanoparticles, nanofibers, carbon nanotubes (CNTs), graphene, titanate nanosheets, and nanocomposites, undergoing extensive investigation for their efficacy in detecting heavy metal ions.

The electrochemical method, exemplified by Anodic Stripping Voltammetry (ASV), emerges as a promising and refined technique for the sensitive detection of minute concentrations of hazardous heavy metal ions, boasting merits including high sensitivity, selectivity, rapid detection capabilities and the capacity for simultaneous detection of multiple heavy metals [20,21].

2.4.3 Semiconductor-based Heavy Metal Ion Sensor

2.4.3.1 Metal Oxide Semiconductors

Nanostructured metal oxides, characterized by superior electron-transfer kinetics and robust adsorption capacities onto the working electrode surface, exhibit proficiency in detecting a broad spectrum of ions; prevalent metal oxides such as ZnO, CuO, Fe_3O_4, SnO_2, ZrO_2, TiO_2, MgO and MnO_2 find widespread application in heavy metal ion sensing, owing to their advantageous traits encompassing biocompatibility, minimal toxicity, and heightened

catalytic efficacy. In a study conducted by Wei et al. [22], they achieved highly selective and sensitive detection of Pb^{2+} and Cd^{2+} ions by creating adsorptive porous magnesium oxide (MgO) nanoflowers. By employing stripping voltammetry analysis, they were able to detect Pb^{2+} ions with a detection limit of 2.1 pM and Cd^{2+} ions with a detection limit of 81 pM. Another recent report by Buica et al. [23] demonstrated an integrated sensing system for the detection of heavy metals such as Cd^{2+}, Pb^{2+}, Hg^{2+} and Cu^{2+}. They utilized Zr/ZrO2-based electrodes and observed enhanced sensitivity rates under UV irradiation. Similarly, Yantasee et al. [24] presented a straightforward method for detecting Pb^{2+} ions in urine using dimercaptosuccinic acid (DMSA) functionalized superparamagnetic Fe_3O_4 nanoparticles. This sensor also exhibited the ability to detect other heavy metals like Cd, Pb, Cu and Ag in natural waters at concentrations below 1 ppb. Gao et al. developed a rapid and direct electrochemical detection method for Arsenic (As) in drinking water, without the need for noble metals [25]. Xie et al. synthesized a graphene-decorated CeO_2 nanocomposite using a hydrothermal approach, demonstrating excellent electrochemical detection of heavy metal ions in aqueous solutions [26]. Zhou et al. reported improved electrochemical sensing performance for heavy metal ions using l-cysteine functionalized $MnFe_2O_4$ mesoporous nanospheres as electrochemical sensors, enabling the identification of Pb^{2+}, Cu^{2+}, Hg^{2+} and Cd^{2+} in aqueous solutions [27]. Wu et al. prepared NiO nanosheets through calcination, achieving promising results for the detection of Hg^{2+} ions, even at low concentrations [28].

2.4.3.2 Transition Metal Dichalcogenides (TMDCs)

Transition Metal Dichalcogenides (TMDCs), having distinctive structural characteristics, constitute a class of two-dimensional layered materials valued for their versatility across a myriad of applications spanning energy storage, thermal management, optoelectronics, catalysis, superconductivity, as well as heavy metal ion detection and gas sensing [29-32]. These materials are composed of hexagonal layers of metal atoms (M), which can be any transition metal element from groups IV-VII B (such as Mo, W, V, Nb, Ta, Ti, Zr, Hf and Re), sandwiched between two layers of chalcogen atoms (X) like S, Se or Te, resulting in a three-layer atomic structure [33]. One of the remarkable features of TMDCs is their tunable bandgap, which plays a crucial role in determining their specific applications. TMDCs exhibit a high surface-to-volume ratio, providing a larger number of active sites on their surfaces for enhanced adsorption capacity, making them suitable for addressing

environmental pollution challenges [34,35]. Rahman et al. achieved the successful synthesis of 1T-WS_2 microflowers using a straightforward hydrothermal method. These micro flowers demonstrated improved sensitivity for detecting ultra-trace levels of Hg^{2+} ions in aqueous solutions, offering high accuracy and reliability. The measured detection limit for Hg^{2+} was approximately 79.8 pM, surpassing the standard permissible limits recommended for drinking water [36]. Yin et al. (2017) demonstrated the selective detection of Cd^{2+} ions using a self-assembled nanocomposite called MoS_2/TMPyP. The nanocomposite exhibited high sensitivity, allowing for the detection of Cd^{2+} ions at lower limits of up to 7.2×10^{-8} mol/L [37]. Li et al. achieved the successful synthesis of flower-like microspheres of WS_2 and WSe_2 using facile and high yield solvothermal methods. These microspheres exhibited remarkable detection capability for Pb^{2+} and Hg^{2+}, highlighting their significant potential for detecting heavy metals even at traceable limits [38].

2.5 Fabrication of sensing layer

In the fabrication of efficient Heavy Metal Ion Sensors, the sensing material plays pivotal role, with nanostructured materials garnering substantial interest of late owing to their exceptional adsorption and catalytic properties.

The synthesis techniques for nanostructured materials can be categorized into two divisions: (i) Top-Down Approaches and (ii) Bottom-Up Approaches. These methods offer diverse approaches to create nanostructured materials with desirable properties for sensing applications.

2.5.1 Top-Down Approaches

Top-down approaches involve the fragmentation or division of bulk materials to obtain nanostructured materials. Different Top-Down Techniques are as follows-

- Mechanical Milling
- LASER Ablation
- Etching
- Sputtering

- Electrospinning
- Lithography

2.5.2 Bottom-Up Approaches

Bottom-Up Synthesis Techniques involve starting with small molecules or atoms and assembling them into larger, more complex molecules or structures through chemical reactions. This approach allows for precise control over the final product's properties and structure. Different Bottom-Up Techniques are as follows-

- Chemical Vapour Deposition (CVD) Technique
- Hydrothermal Method
- Solvothermal Method
- Chemical Bath Deposition (CBD) Technique
- Sol-Gel Method

REFERENCES:

1. F. Habashi, "Gmelin and his Handbuch," Bulletin for the History of Chemistry, vol. 34, no. 2, p. 30, 2009.
2. O. Pourret, J.-C. Bollinger, and A. Hursthouse, "Heavy metal: a misused term?," Acta Geochimica, vol. 40, pp. 466-471, 2021.
3. J. H. Duffus, "" Heavy metals" a meaningless term?(IUPAC Technical Report)," Pure and applied chemistry, vol. 74, no. 5, pp. 793-807, 2002.
4. N. P. Raval, P. U. Shah, and N. K. Shah, "Adsorptive removal of nickel (II) ions from aqueous environment: A review," Journal of Environmental Management, vol. 179, pp. 1-20, 2016.
5. P. B. Tchounwou, C. Yedjou, A. Patlolla, D. Sutton, and A. Luch, "Molecular, clinical and environmental toxicology," Molecular, Clinical and Environmental Toxicology, vol. 3, pp. 133-164, 2012.
6. G. WHO, "Guidelines for drinking-water quality," World health organization, vol. 216, pp. 303-304, 2011.
7. H. Bradl, "Heavy metals interaction in the environment; origin, interactions, and remediation," ed: London Academic Press (6), 2002.
8. J. E. Fergusson and F. P. Prucha, The heavy elements: chemistry, environmental impact and health effects. Pergamon press Oxford, 1990.
9. M. B. Gumpu, S. Sethuraman, U. M. Krishnan, and J. B. B. Rayappan, "A review on detection of heavy metal ions in water–an electrochemical approach," Sensors and actuators B: chemical, vol. 213, pp. 515-533, 2015.

10. R. Mohamed, A. Abdel-Lateef, H. Mahmoud, and A. Helal, "Determination of trace elements in water and sediment samples from Ismaelia Canal using ion chromatography and atomic absorption spectroscopy," Chemical Speciation & Bioavailability, vol. 24, no. 1, pp. 31-38, 2012.
11. L. Eddaif, A. Shaban, J. Telegdi, and I. Szendro, "A piezogravimetric sensor platform for sensitive detection of lead (ii) ions in water based on calix [4] resorcinarene macrocycles: synthesis, characterization and detection," Arabian Journal of Chemistry, vol. 13, no. 2, pp. 4448-4461, 2020.
12. M. Batsala, B. Chandu, B. Sakala, S. Nama, and S. Domatoti, "Inductively coupled plasma mass spectrometry (ICP-MS)," Int J Res Pharm Chem, vol. 2, no. 3, pp. 671 680, 2012.
13. F. Zhao, Z. Chen, F. Zhang, R. Li, and J. Zhou, "Ultra-sensitive detection of heavy metal ions in tap water by laser-induced breakdown spectroscopy with the assistance of electrical-deposition," Analytical Methods, vol. 2, no. 4, pp. 408-414, 2010.
14. G. WHO, "Hardness in Drinking-water: background document for development of WHO guidelines for drinking-water quality," ed: World Health Organization Geneva, 2011.
15. L. Borgese, A. Zacco, E. Bontempi, M. Pellegatta, L. Vigna, and L. Patrini, "L. Riboldi, Rubino FM, Depero LE Use of total reflection X-ray fluorescence (TXRF) for the evaluation of heavy metal poisoning due to the improper use of a traditional ayurvedic drug," J. Pharm. Biomed. Anal, vol. 52, pp. 787-790, 2010.
16. C. W. Commission, "Status of trace and toxic metals in Indian Rivers," Ministry of Jal Shakti, Department of Water Resources, River Development, and Ganga Rejuvenation: New Delhi, India, 2019.

17. C. Sarzanini and M. C. Bruzzoniti, "Metal species determination by ion chromatography," TrAC Trends in Analytical Chemistry, vol. 20, no. 6-7, pp. 304 310, 2001.
18. Y. Yang, S. Matsubara, M. Nogami, J. Shi, and W. Huang, "One-dimensional self assembly of gold nanoparticles for tunable surface plasmon resonance properties," Nanotechnology, vol. 17, no. 11, p. 2821, 2006.
19. M. Li, X. Zhou, W. Ding, S. Guo, and N. Wu, "Fluorescent aptamer-functionalized graphene oxide biosensor for label-free detection of mercury (II)," Biosensors and Bioelectronics, vol. 41, pp. 889-893, 2013.
20. C. Gao, X.-Y. Yu, R.-X. Xu, J.-H. Liu, and X.-J. Huang, "AlOOH-reduced graphene oxide nanocomposites: one-pot hydrothermal synthesis and their enhanced electrochemical activity for heavy metal ions," ACS applied materials & interfaces, vol. 4, no. 9, pp. 4672-4682, 2012.
21. A. Economou and P. Fielden, "Mercury film electrodes: developments, trends and potentialities for electroanalysis," Analyst, vol. 128, no. 3, pp. 205-213, 2003.
22. Y. Wei, R. Yang, X.-Y. Yu, L. Wang, J.-H. Liu, and X.-J. Huang, "Stripping voltammetry study of ultra-trace toxic metal ions on highly selectively adsorptive porous magnesium oxide nanoflowers," Analyst, vol. 137, no. 9, pp. 2183-2191, 2012.
23. G.-O. Buica, A. B. Stoian, C. Manole, I. Demetrescu, and C. Pirvu, "Zr/ZrO2 nanotube electrode for detection of heavy metal ions," Electrochemistry Communications, vol. 110, p. 106614, 2020.
24. W. Yantasee et al., "Direct detection of Pb in urine and Cd, Pb, Cu, and Ag in natural waters using electrochemical sensors immobilized with DMSA functionalized magnetic nanoparticles," Analyst, vol. 133, no. 3, pp. 348-355, 2008.

25. C. Gao, X.-Y. Yu, S.-Q. Xiong, J.-H. Liu, and X.-J. Huang, "Electrochemical detection of arsenic (III) completely free from noble metal: Fe3O4 microspheres room temperature ionic liquid composite showing better performance than gold," Analytical chemistry, vol. 85, no. 5, pp. 2673-2680, 2013.
26. Y.-L. Xie, S.-Q. Zhao, H.-L. Ye, J. Yuan, P. Song, and S.-Q. Hu, "Graphene/CeO2 hybrid materials for the simultaneous electrochemical detection of cadmium (II), lead (II), copper (II), and mercury (II)," Journal of Electroanalytical Chemistry, vol. 757, pp. 235-242, 2015.
27. S.-F. Zhou et al., "Individual and simultaneous electrochemical detection toward heavy metal ions based on L-cysteine modified mesoporous MnFe2O4 nanocrystal clusters," Journal of Alloys and Compounds, vol. 721, pp. 492-500, 2017.
28. Z. Wu, L. Jiang, Y. Zhu, C. Xu, Y. Ye, and X. Wang, "Synthesis of mesoporous NiO nanosheet and its application on mercury (II) sensor," Journal of Solid State Electrochemistry, vol. 16, pp. 3171-3177, 2012.
29. Y.-P. Gao, X. Wu, K.-J. Huang, L.-L. Xing, Y.-Y. Zhang, and L. Liu, "Two dimensional transition metal diseleniums for energy storage application: a review of recent developments," CrystEngComm, vol. 19, no. 3, pp. 404-418, 2017.
30. J. Lu et al., "Evidence for two-dimensional Ising superconductivity in gated MoS2," Science, vol. 350, no. 6266, pp. 1353-1357, 2015.
31. R. Kumar, N. Goel, and M. Kumar, "UV-activated MoS2 based fast and reversible NO2 sensor at room temperature," ACS sensors, vol. 2, no. 11, pp. 1744-1752, 2017.
32. A. Nigam et al., "Real time detection of Hg2+ ions using MoS2 functionalized AlGaN/GaN high electron mobility transistor for water quality monitoring," Sensors and Actuators B: Chemical, vol. 309, p. 127832, 2020.

33. R. Kappera et al., "Phase-engineered low-resistance contacts for ultrathin MoS2 transistors," Nature materials, vol. 13, no. 12, pp. 1128-1134, 2014.
34. X. Zhang, S. Y. Teng, A. C. M. Loy, B. S. How, W. D. Leong, and X. Tao, "Transition metal dichalcogenides for the application of pollution reduction: A review," Nanomaterials, vol. 10, no. 6, p. 1012, 2020.
35. H. Wang, C. Li, P. Fang, Z. Zhang, and J. Z. Zhang, "Synthesis, properties, and optoelectronic applications of two-dimensional MoS2 and MoS2-based heterostructures," Chemical Society Reviews, vol. 47, no. 16, pp. 6101-6127, 2018.
36. M. T. Rahman et al., "Metallic 1T phase tungsten disulfide microflowers for trace level detection of Hg2+ ions," Advanced Sustainable Systems, vol. 4, no. 9, p. 2000068, 2020.
37. W. Yin et al., "MoS2-nanosheet-assisted coordination of metal ions with porphyrin for rapid detection and removal of cadmium ions in aqueous media," ACS Applied Materials & Interfaces, vol. 9, no. 25, pp. 21362-21370, 2017.
38. S. M. Rosolina, S. A. Bragg, R. Ouyang, J. Q. Chambers, and Z.-L. Xue, "Highly sensitive detection of hexavalent chromium utilizing a sol-gel/carbon nanotube modified electrode," Journal of Electroanalytical Chemistry, vol. 781, pp. 120-125, 2016.

CHAPTER 3

3. Fabrication of Gated Voltage Assisted Zinc Oxide Nanowire-based n-n^+ Heterostructure Device

In this chapter the experiments involved in the synthesis procedure of the sensing material is provided. As well as this chapter covers the variation in synthesis procedure and Field Emission Scanning Electron Microscope (FESEM) images, X-Ray Diffraction (XRD) plots, Diffuse Reflectance Spectroscopy (DRS) data observed in those variations. Moreover the experimental setup for Gated Voltage Assisted Zinc Oxide Nanowire-based n-n^+ Heterostructure is explained. Finally the Current (I) – Voltage (V) Characteristics Curve observed in bare device and its probable mechanism is included.

3.1 Synthesis of Sensing Material

3.1.1 Chemicals and Instruments

Chemicals used in the synthesis procedure are-

1. Zinc Nitrate Hexahydrate : $Zn(NO_3)_2.6H_2O$ [Molecular Weight-297.49]
2. 25% Ammonia Solution : NH_4OH [Molecular Weight-35.05]
3. Hexamethylenetetramine (HMTA) : $C_6H_{12}N_4$ [Molecular Weight-140.19]

{all chemicals are purchased from Sigma-Aldrich}



Figure 3.1(a): Zinc Nitrate Hexahydrate



Figure 3.1(b): Hexamethylenetetramine (HMTA)



Figure 3.1(c): 25% Ammonia Solution

The Instruments involved in the synthesis procedure are-

1. Magnetic Stirrer with Hot Plate
2. Regulated DC Power Supply



Figure 3.2(a): Magnetic Stirrer with Hot Plate

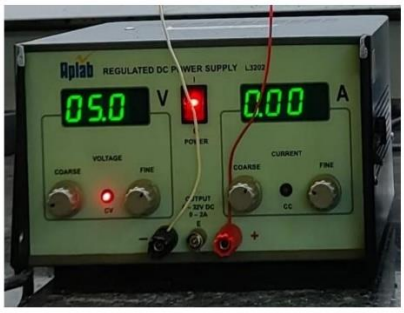


Figure 3.2(b): Regulated DC Power Supply

3.1.2 Synthesis Procedure

In this work, p-type Silicon (100) wafer has been used as a substrate. The p-Si (100) substrates were cleaned using the following steps-

- Atfirst Piranha Solution was prepared. 6mL Sulphuric Acid (H_2SO_4) was poured into 6mL Hydrogen Peroxide (H_2O_2) drop by drop slowly to make a 1:1 solution of H_2SO_4 and H_2O_2. This is a highly exothermic reaction. The solution was used for further proceedings until it calm down. Then the wafers were placed in the Piranha Solution for 1 hour or till the effervescence clears. After that the wafers were removed from the solution and cleaned using De-ionized Water (DI Water) to get rid of any Piranha residues.
- Secondly a 1:10 solution of Hydrofluoric Acid (HF) in DI Water was made. The wafers were poured into it to remove any oxide on the surface [HF handling gloves and Teflon labwares were used while doing this]. The wafers were kept in the solution for about a minute. Finally the wafers were removed from the solution, cleaned using DI Water and let it dry.

Silver Paste was deposited on both sides of the p-Si (100) substrate and heated at 150° C temperature for 1hour in the Hot Air Oven. It takes nearly 1.5-2hours to cool down naturally inside the Hot Air Oven. Then the substrate was taken out of the Hot Air Oven and let it cool down at room temperature for 10-15 minutes. This Silver Paste deposition was done to have a metal contact with the wires which will be connected with the positive and negative port of the Regulated DC Power Supply while performing the voltage-assisted growth of Zinc Oxide Nanowire over the p-Si (100) substrate. The substrate was ready for further experiments.

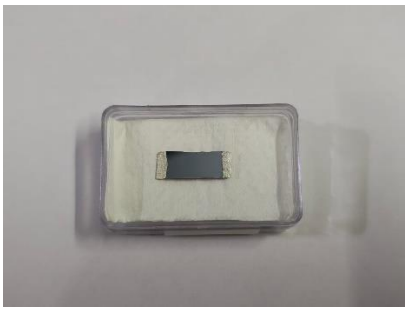


Figure 3.3: Silver Paste deposited p-Si (100) substrate

Double Step Chemical Bath Deposition (CBD) Technique for the synthesis of ZnO Nanowire:

Growth of ZnO Nanowires on the p-Si (100) substrate can be explained in the following two steps-

(a) Step 1: Nucleation of ZnO Seed Layer
(b) Step 2: Synthesis of ZnO Nanowire

- ***Nucleation of ZnO Seed Layer:***

The ZnO seed layer growth process initiates with the preparation of a precursor solution with 5mM of Zinc Nitrate Hexahydrate [$Zn(NO_3)_2.6H_2O$] dissolved in 100mL DI water. The precursor solution was stirred at 120 rpm and the solution temperature was allowed to reach to 60°C. The sample was vertically placed into the precursor solution in such a way that the

negative terminal dipped into the solution and the positive terminal was kept outside under the assistance of a constant DC bias as depicted in the Figure 3.4. After attaining the required temperature, 8mL of 25% ammonia is added to the solution and the colour of the solution converts to milky white. This process was carried out for 30 minutes keeping the temperature of the solution constant at 90°C for the nucleation of ZnO seed layer. Once the nucleation is complete, the ZnO seed layer deposited p-Si (100) substate was taken out from the solution and dipped into DI water.

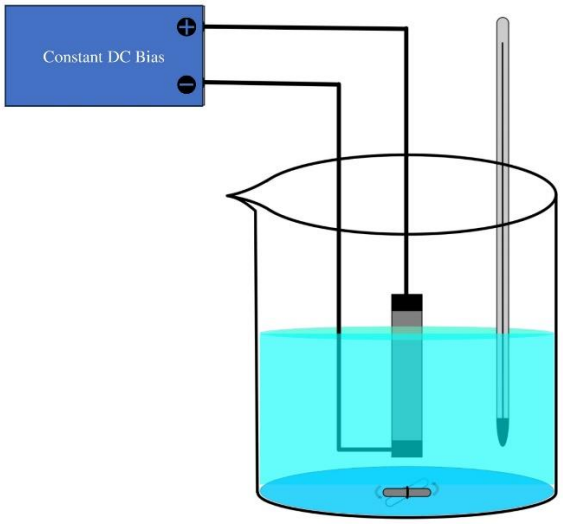


Figure 3.4: Schematic Diagram of the Device submerged in the precursor solution

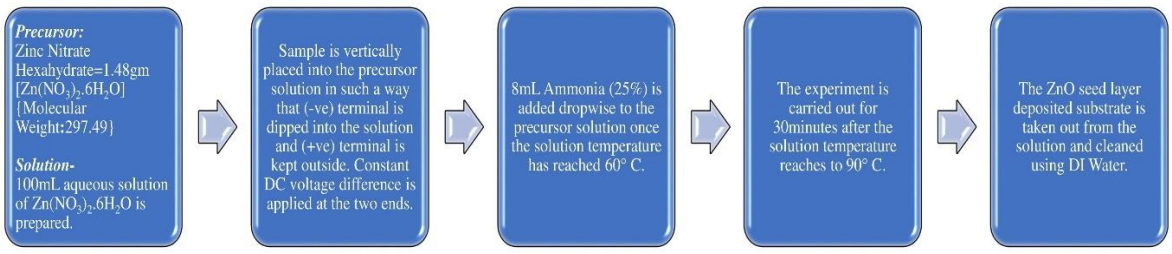


Figure 3.5: Flow Diagram for the Nucleation of ZnO Seed Layer

- ***Synthesis of ZnO Nanowire:***

The growth of ZnO Nanowire was performed by preparing a solution of 2.5mM Zinc Nitrate Hexahydrate [$Zn(NO_3)_2.6H_2O$] dissolved in 50 mL DI water. Another solution was prepared separately by using 2.5mM Hexamethylenetetramine (HMTA) in 50 mL DI water. Both solutions were mixed and ZnO seed layer grown p-Si (100) substrate was placed vertically into the solution following the similar configuration, under the assistance of a constant DC bias. Temperature of the solution was increased up to 90 °C to produce Zn^{2+} and OH^- ions which commenced the growth of ZnO Nanowires. The deposition was conducted for 2hours to grow the ZnO Nanowires. The chemical reactions which were associated with the growth of ZnO Nanowires are shown below-

$$C_6H_{12}N_4 + 6H_2O \rightarrow 6CH_2O + 4NH_3$$

$$NH_3 + H_2O \rightarrow NH_4^+ + OH^-$$

$$Zn^{2+} + 4NH_3 \rightarrow Zn(NH_3)_4^{2+}$$

$$Zn(NH_3)_4^{2+} + 4OH^- \rightarrow Zn(OH)_4^{2-} + 4NH_3$$

$$Zn(NO_3)_2 + 2NH_4 + 2OH^- \rightarrow 2NH_4(NO_3) + Zn(OH)_2$$

$$Zn^{2+} + 4OH^- \rightarrow Zn(OH)_4^{2-}$$

$$Zn(OH)_4^{2-} \rightarrow Zn(OH)_2 + 2OH^-$$

$$Zn(OH)_2 \rightarrow ZnO + H_2O$$

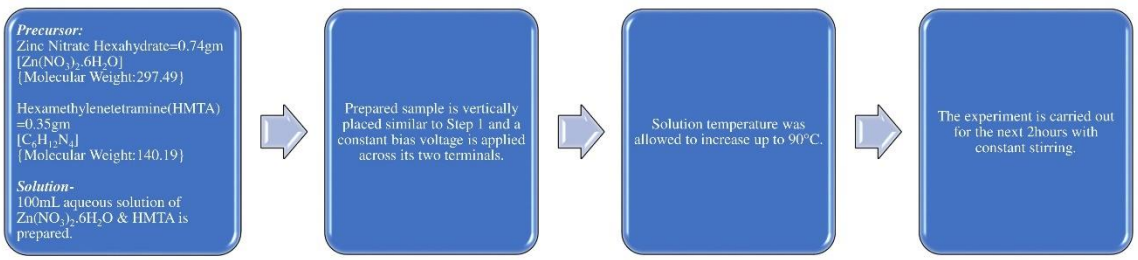


Figure 3.6: Flow Diagram for the Synthesis of ZnO Nanowire

At the initial stage the hydration of HMTA occurs at 60 °C temperature, producing Formaldehyde (CH_2O) which undergoes instantaneous evaporation. Ammonia (NH_3) is another product of this reaction which promotes the formation of ammonium cation NH_4^+ by protonation of NH_3. These reactions release OH^- ions in the precursor solution slowly. Zn^{2+} ions react with NH_3 to produce tetraamine zinc species. The $Zn(NH_3)_4^{2+}$ is transformed to $Zn(OH)_4^{2-}$ through a subsequent reaction in the presence of hydroxyl ions, since this form is more stable than amine complexes. $NH_4(NO_3)$ is then formed to maintain the pH level of the aqueous solution at supersaturating conditions. Zn^{2+} ions react with OH^- ions present in the solution, with the interactions leading to the formation of zinc complex. $[Zn(OH)_4]^{2-}$ ions are thermally decomposed and wurtzite ZnO is nucleated by self-orientation mechanism. The kinematics of Zn^{2+} and OH^- ions near the substrate surfaces are controlled by the applied electric field during the growth. [1-9]

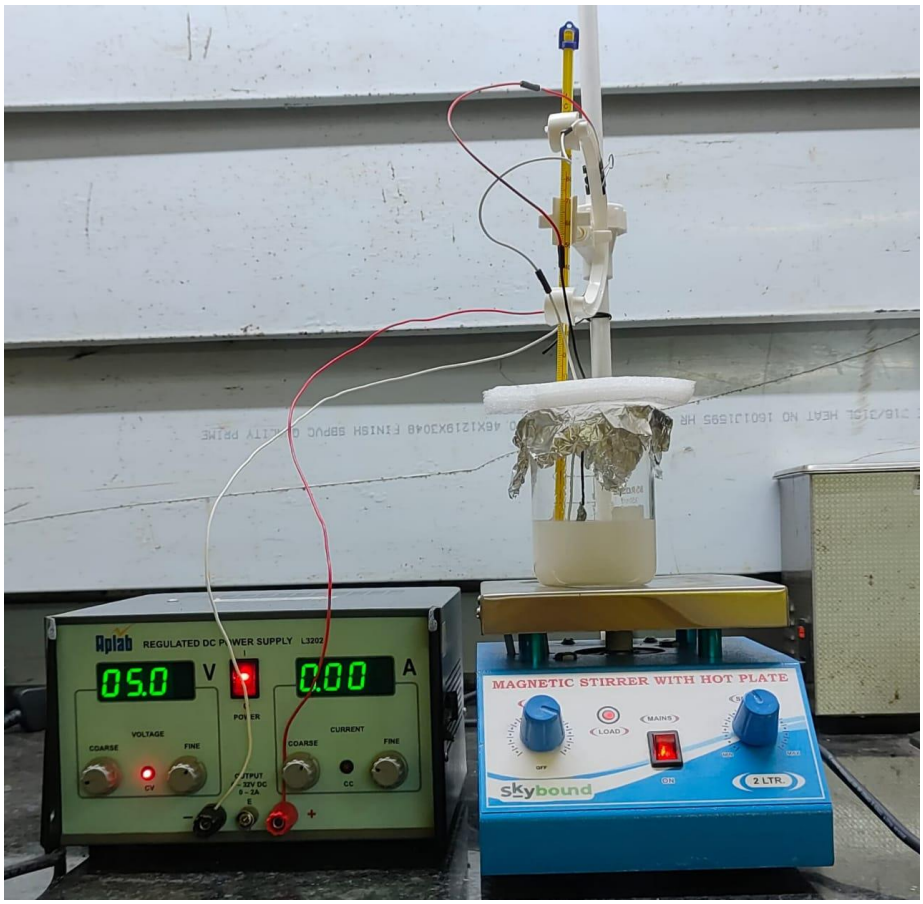


Figure 3.7: Experimental Setup for the growth of ZnO Nanowire

For ZnO Nanowire growth Zinc Nitrate Hexahydrate [$Zn(NO_3)_4.6H_2O$] and Hexamethylenetetramine i.e. HMTA [$C_6H_{12}N_4$] were used as precursors. During the reaction, more number of Zn^{2+} ions were getting accumulated towards negative terminal and comparatively less number of Zn^{2+} ions were getting accumulated towards positive terminal. A concentration gradient was observed. So, towards negative terminal More n-type Region and towards positive terminal Less n-type Region were observed. Therefore, a Zinc Oxide Nanowire based n-n^+ heterostructure was formed.

3.1.3 Variation in Synthesis Procedure

Keeping the synthesis procedure same, by only varying the DC Bias Voltage four set of Zinc Oxide Nanowire (NW) based n-n^+ heterostructure devices were prepared-

(1) ZnO NW based device under 2.5V Bias Voltage
(2) ZnO NW based device under 5V Bias Voltage
(3) ZnO NW based device under 7.5V Bias Voltage
(4) ZnO NW based device under 10V Bias Voltage

The Field Emission Scanning Electron Microscope (FESEM) images, X-Ray Diffraction (XRD) plots, Diffuse Reflectance Spectroscopy (DRS) data observed in these variations are discussed in the following sections.

3.1.4 FESEM Images observed in those variation

Figure 3.8 showcases the Field Emission Scanning Electron Microscope (FESEM) images of Zinc Oxide Nanowire based n-n^+ heterostructure device under 5V Bias Voltage towards Less n-type Region and towards More n-type Region.

The ionic concentrations were different in different regions. Zn^{2+} ions react with OH^- ions present in the solution and their interactions leading to the formation of zinc complex. $[Zn(OH)_4]^{2-}$ ions are thermally decomposed. As a result, wurtzite ZnO is nucleated by self-orientation mechanism. Since the number of Zn^{2+} ions are more towards More n-type Region,

hence the formation of zinc complex is more and the nucleation rate of wurtzite ZnO is more in this region compared to Less n-type Region. Therefore, we got a variation in morphology in these two regions. Further, it can also be said that due to the presence of external field on substrate the pH of both the regions may vary. As it is well established that the pH of the solution is one of the major controlling factor for ZnO growth process. That may be another reason for the variation in morphology in these two regions.

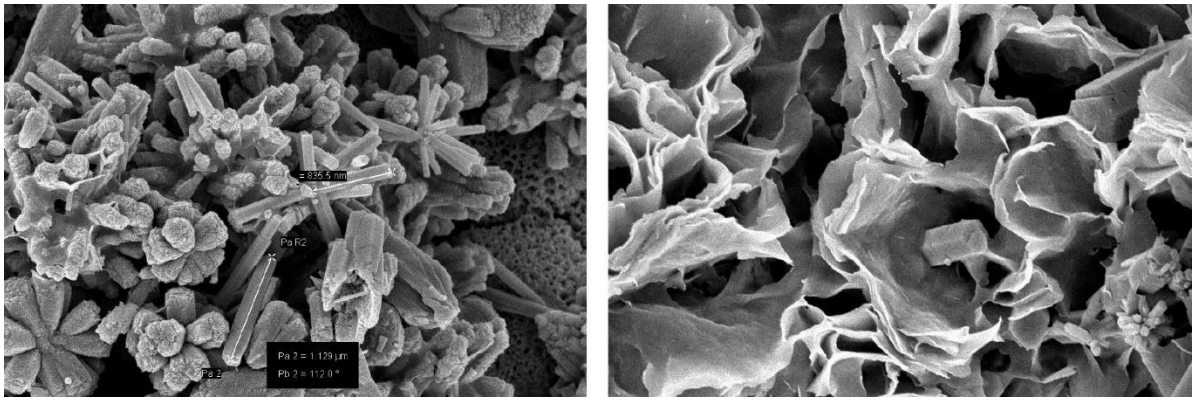


Figure 3.8: FESEM Images of ZnO Nanowire based n-n^+ heterostructure devices (Less n-type Region in the left side & More n-type Region in the right side)

3.1.5. X-Ray Diffraction (XRD) Analysis

X-Ray Diffraction (XRD) was performed for the morphological and structural analysis of the above-mentioned devices. From Scherrer Formula and Williamson-Hall Plot the crystallite sizes were determined and compared.

Figure 3.9 (a) to (h) depict the XRD spectrum of ZnO nanowires. Distinct peaks were observed at 31.88°, 34.59°, 36.31°, 47.70°, 56.56° and 62.99° corresponding to the (100), (002), (101), (102), (110) and (103) planes of hexagonal ZnO (JCPDS card no. 36-1451).

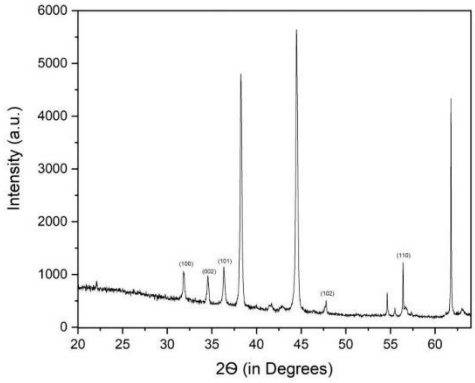


Figure 3.9 (a): XRD Spectrum of Less n-type Region in ZnO Nanowire under 2.5V Bias Voltage

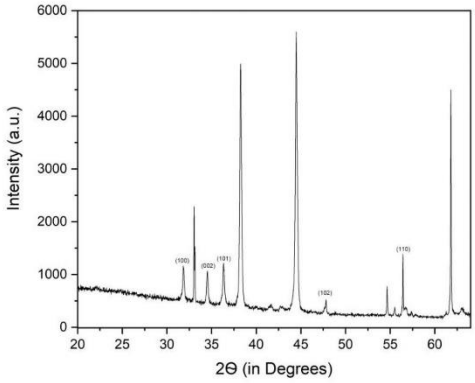


Figure 3.9 (b): XRD Spectrum of More n-type Region in ZnO Nanowire under 2.5V Bias Voltage

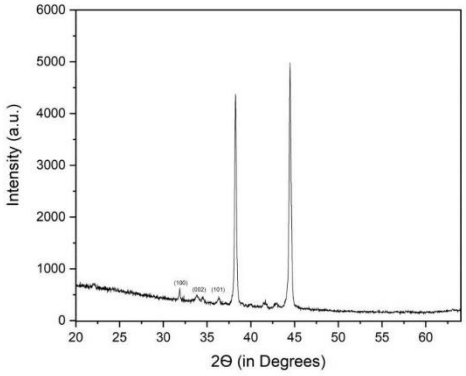


Figure 3.9 (c): XRD Spectrum of Less n-type Region in ZnO Nanowire under 5V Bias Voltage

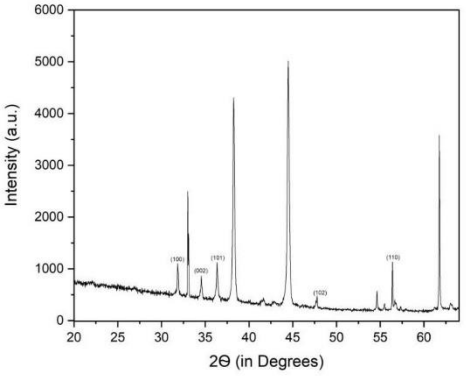


Figure 3.9 (d): XRD Spectrum of More n-type Region in ZnO Nanowire under 5V Bias Voltage

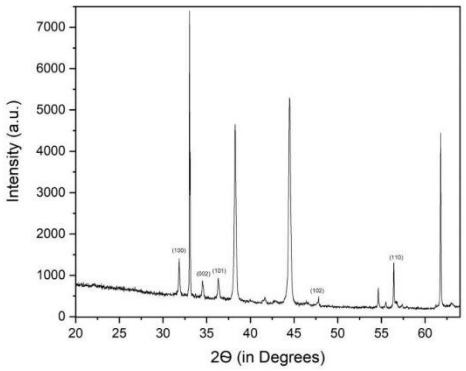


Figure 3.9 (e): XRD Spectrum of Less n-type Region in ZnO Nanowire under 7.5V Bias Voltage

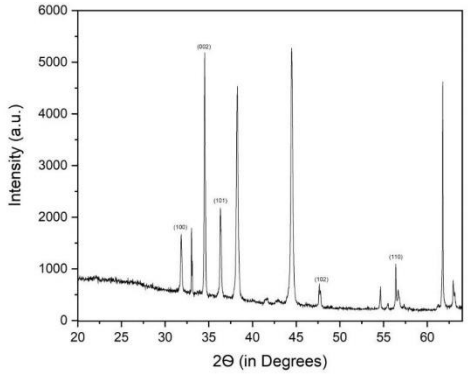


Figure 3.9 (f): XRD Spectrum of More n-type Region in ZnO Nanowire under 7.5V Bias Voltage

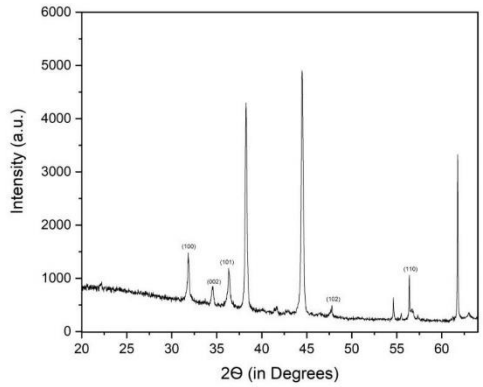


Figure 3.9 (g): XRD Spectrum of Less n-type Region in ZnO Nanowire under 10V Bias Voltage

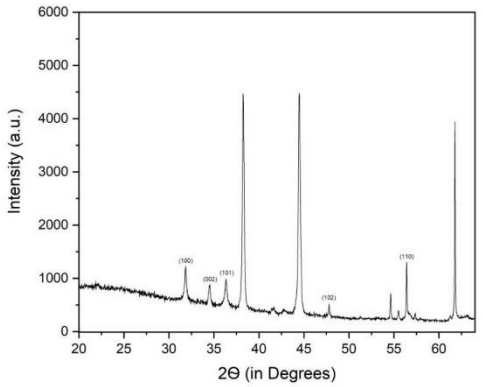


Figure 3.9 (h): XRD Spectrum of More n-type Region in ZnO Nanowire under 10V Bias Voltage

Among all the XRD Plots that have been shown above, a variation in intensities of the diffraction peaks between Less n-type Region and More n-type Region is observed. For all the devices the intensity of diffraction peak is more towards the More n-type Region. Moreover with the increase in Bias Voltage i.e. from 2.5V to 10V, an increase in intensity in all the diffraction peaks for all the devices is observed.

For an example, the X-Ray Diffraction Spectrum of ZnO NW under 7.5V Bias Voltage for both Less n-type Region and More n-type Region is shown in Figure 3.10. The difference between the diffraction peak intensities of 268a.u. for (100) plane in those two regions is observed.

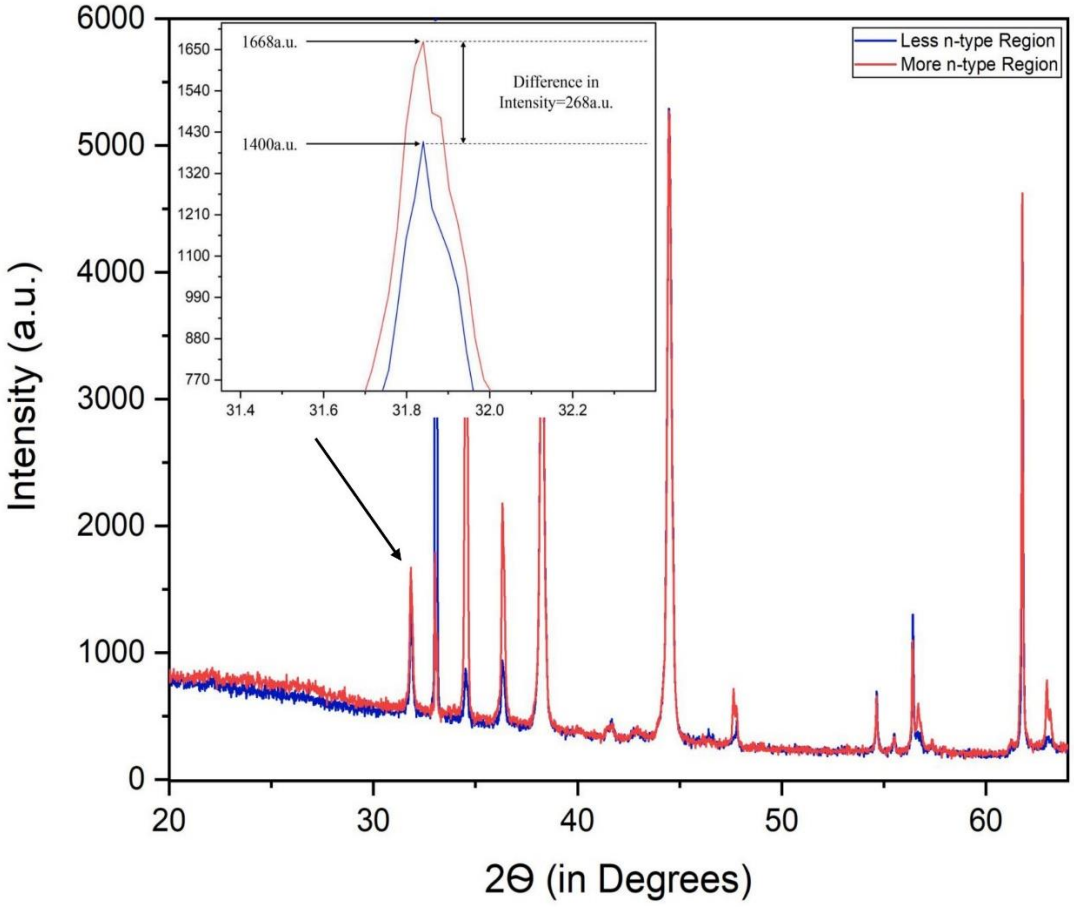


Figure 3.10: Variation in Diffraction Peak intensities in different regions for ZnO NW under 7.5V Bias Voltage

The difference between the intensities of diffraction peaks for different planes in all the devices are shown in Table 3.1.

Table 3.1: Intensities of Diffraction Peaks for Different Planes in all the devices

Device	(100) plane	(002) plane	(101) plane	(102) plane	(110) plane
Less n-type region in ZnO NW under 2.5V Bias Voltage	1068 a.u.	979 a.u.	1148 a.u.	509 a.u.	1225 a.u.
More n-type region in ZnO NW under 2.5V Bias Voltage	1168 a.u.	1068 a.u.	1216 a.u.	525 a.u.	1388 a.u.
Less n-type region in ZnO NW under 5V Bias Voltage	633 a.u.	470 a.u.	472 a.u.	X	X
More n-type region in ZnO NW under 5V Bias Voltage	1107 a.u.	870 a.u.	1127 a.u.	479 a.u.	1133 a.u.
Less n-type region in ZnO NW under 7.5V Bias Voltage	1400 a.u.	876 a.u.	938 a.u.	493 a.u.	1097 a.u.
More n-type region in ZnO NW under 7.5V Bias Voltage	1668 a.u.	5186 a.u.	2177 a.u.	717 a.u.	1304 a.u.
Less n-type region in ZnO NW under 10V Bias Voltage	1232 a.u.	854 a.u.	990 a.u.	494 a.u.	1062 a.u.
More n-type region in ZnO NW under 10V Bias Voltage	1478 a.u.	889 a.u.	1191 a.u.	521 a.u.	1311 a.u.

These variations in diffraction peak intensities can be explained from the concept of Structure Factor. The Structure Factor [F(hkl)] plays a crucial role in the determination of diffraction peak intensity observed in X-Ray Diffraction (XRD) patterns. The intensity [I(hkl)] of a diffraction peak corresponding to a set of Miller Indices (hkl) is proportional to the square of the magnitude of Structure Factor [F(hkl)].

$$I(hkl) \propto |F(hkl)|^2$$

That means if the Diffraction Peak Intensity of a certain region is high then the Structure Factor of that region is large. From the XRD Spectrums of the above-mentioned devices it can be concluded that the Structure Factor is High towards the More n-type Regions compared to Less n-type Regions. Moreover, the Structure Factor in the device increases while increasing the Bias Voltage. [4,5]

Particle Size of different regions of the as-prepared device under different Bias Voltage are calculated using Scherrer Formula and the comparison of that with the particle size determined from Williamson-Hall Plot is shown in Table 3.2

From the comparison table it can be observed that the particle size is more towards the Less n-type Region and it is less towards the More n-type Region. This variation arised because towards Less n-type Region the peak broadening is less and towards More n-type Region the peak broadening is more. Basically it signifies that the sample is not uniform. This inhomogeneity can affect the device's overall properties.

Table 3.2: Comparison of Particle Size from Scherrer Formula and from Williamson-Hall Plot

Device	Particle Size from Scherrer Formula (in nm)	Particle Size from Williamson-Hall Plot (in nm)
Less n-type Region in ZnO Nanowire under 2.5V Bias Voltage	134.2	129.83
More n-type Region in ZnO Nanowire under 2.5V Bias Voltage	130.8	124.42
Less n-type Region in ZnO Nanowire under 5V Bias Voltage	141.03	137.9
More n-type Region in ZnO Nanowire under 5V Bias Voltage	139.01	135.4
Less n-type Region in ZnO Nanowire under 7.5V Bias Voltage	135.6	136.31
More n-type Region in ZnO Nanowire under 7.5V Bias Voltage	131.76	134.78
Less n-type Region in ZnO Nanowire under 10V Bias Voltage	137.87	138.93
More n-type Region in ZnO Nanowire under 10V Bias Voltage	134.92	135.71

3.1.6 Diffuse Reflectance Spectroscopy (DRS) Data observed in those variations

Diffuse Reflectance Spectroscopy (DRS) is performed for all the devices. DRS measures the amount of light reflected by a sample across a range of wavelengths. From the DRS Data the Band Gap Energy in all the regions for all the devices under different Bias Voltage is measured using Tauc's Method and the corresponding data are shown in the Table 3.3.

Table 3.3: Band Gap Energy in different regions of the devices

Device	Band Gap Energy towards Less n-type Region (in eV)	Band Gap Energy towards More n-type Region (in eV)
ZnO Nanowire under 2.5V Bias Voltage	3.305	3.318
ZnO Nanowire under 5V Bias Voltage	3.291	3.344
ZnO Nanowire under 7.5V Bias Voltage	3.307	3.351
ZnO Nanowire under 10V Bias Voltage	3.273	3.3507

From the above table it can be observed that the Band Gap Energy is less towards Less n-type Region and it is more towards More n-type Region for all the devices.

According to Quantum Confinement Effect, the Band Gap Energy of a semiconductor is inversely proportional to the square of its size i.e.

$$E_g \propto (1/L)^2$$

where, E_g= Band Gap Energy of the semiconductor

L=Size of the semiconductor

Hence, it can be stated that the size of the particles is more towards the Less n-type Region and the size is less towards the More n-type Region, which correlates with the data for particle size observed from Scherrer Formula and Williamson-Hall Plot shown in Table 3.2.

3.2 Experimental Setup for Gated Voltage Assisted Zinc Oxide Nanowire-based n-n^+ Heterostructure

To observe the variation in Current(I)-Voltage(V) Characteristics and the response towards different heavy metal ions, a third terminal is connected in the ZnO Nanowire-based n-n^+ Heterostructure Device using the Probe Station.

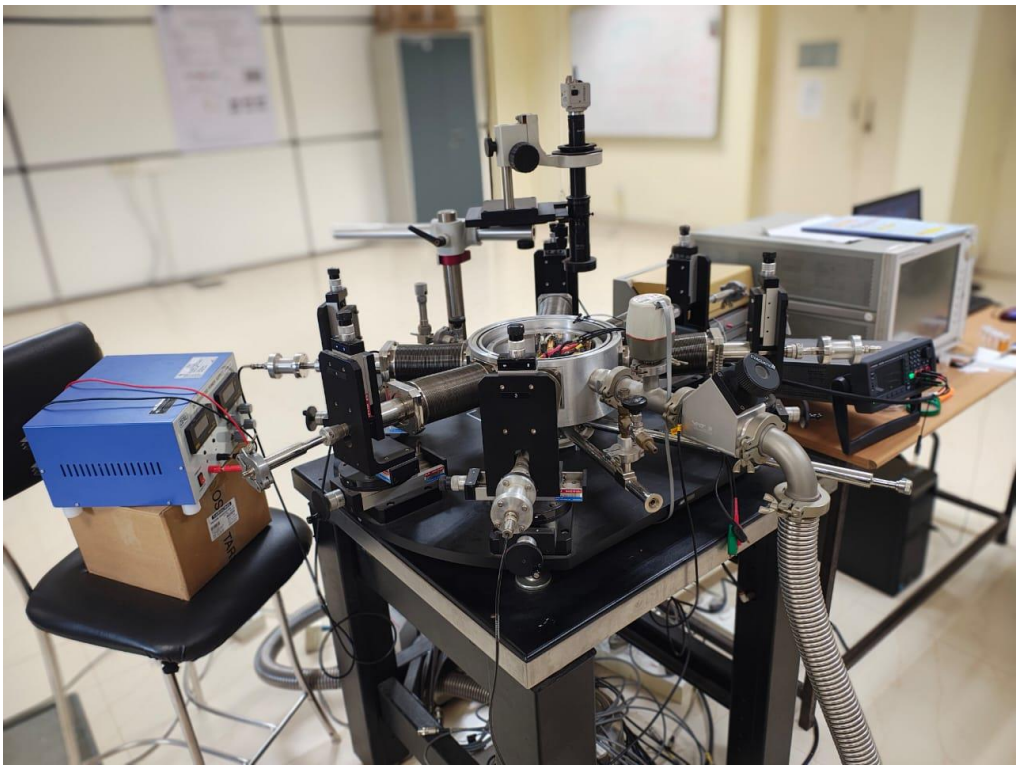


Figure 3.11: Probe Station used for Experiment

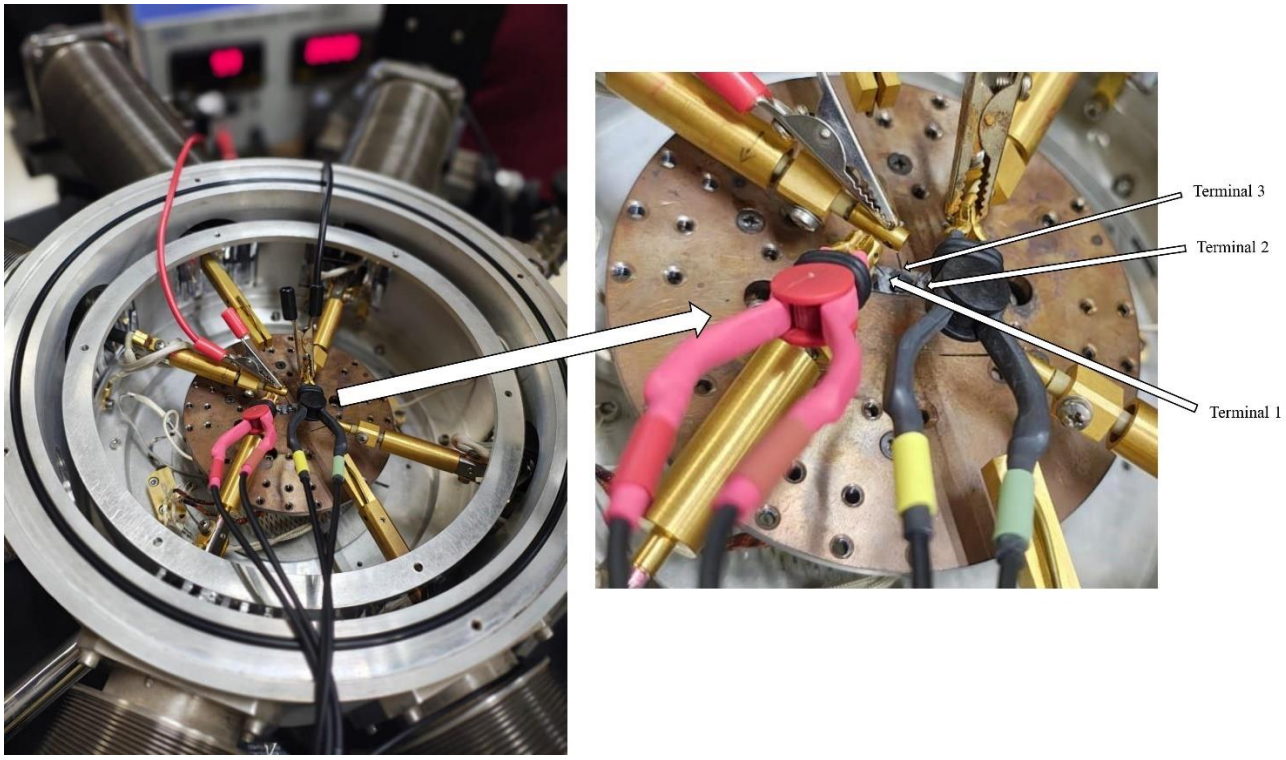


Figure 3.12: Three Terminal arrangement in the device inside the Probe Station

3.2.1 Current(I)-Voltage(V) Characteristics observed in Bare Device

For finding the I-V Characteristics of the device the Probe Station is connected with the Keysight Source Measurement Unit (SMU) and using the Keysight B2900 Quick IV Measurement Software the corresponding data are collected. The same experimental setup is used for the heavy metal sensing purpose also.

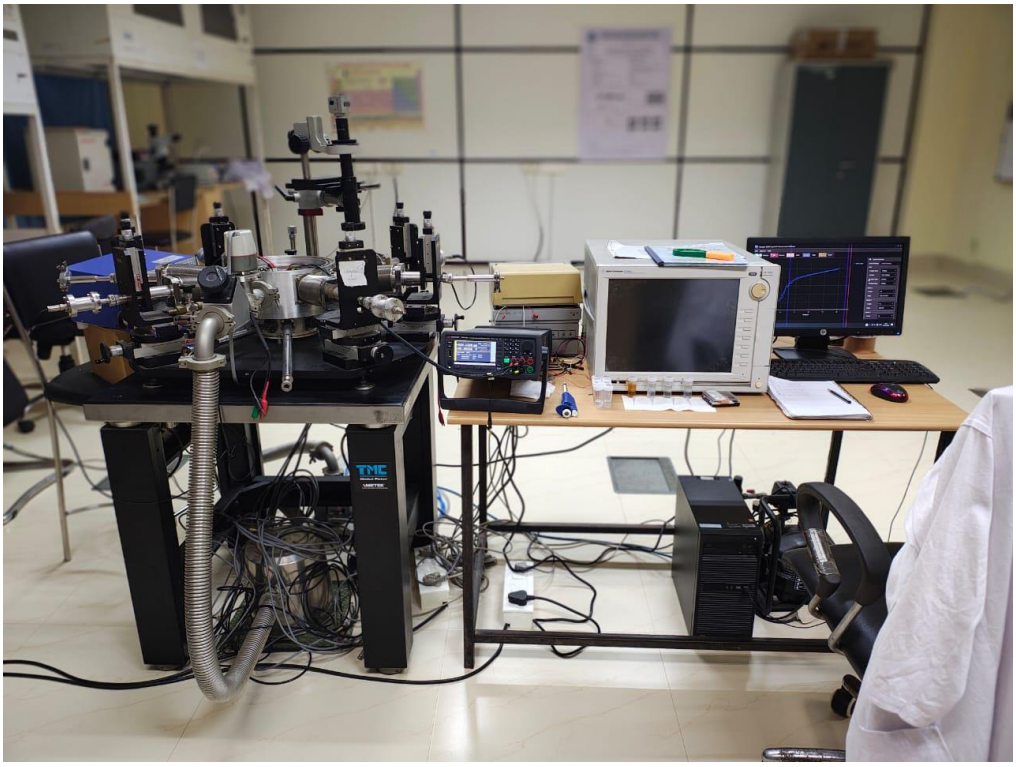


Figure 3.13: Entire Experimental Setup for finding the I-V Characteristics of the Three-Terminal Device

- **I-V Characteristics observed in Two Terminal Device**

Atfirst, the Current(I)-Voltage(V) Characteristics are measured for all the devices under bare condition when the third terminal was not connected. Figure 3.14 (a)-(d) showcases all those IV Characteristic Curves.

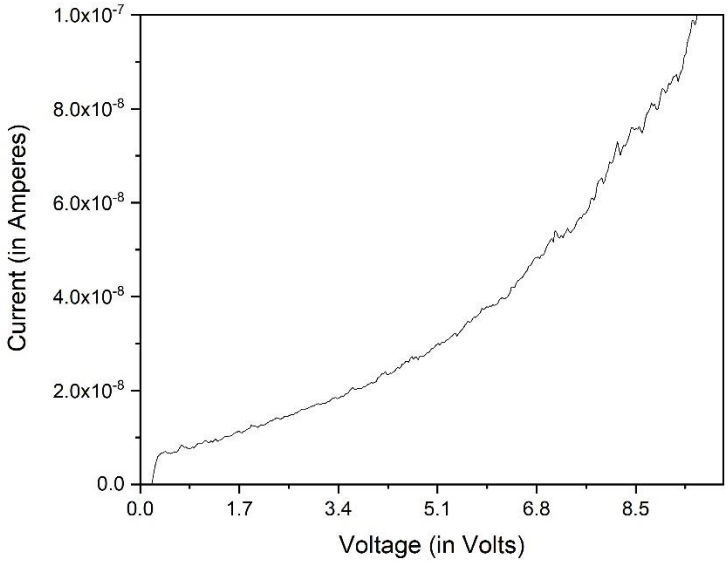


Figure 3.14(a): IV Characteristics of Two Terminal ZnO NW-based Device under 2.5V Bias Voltage

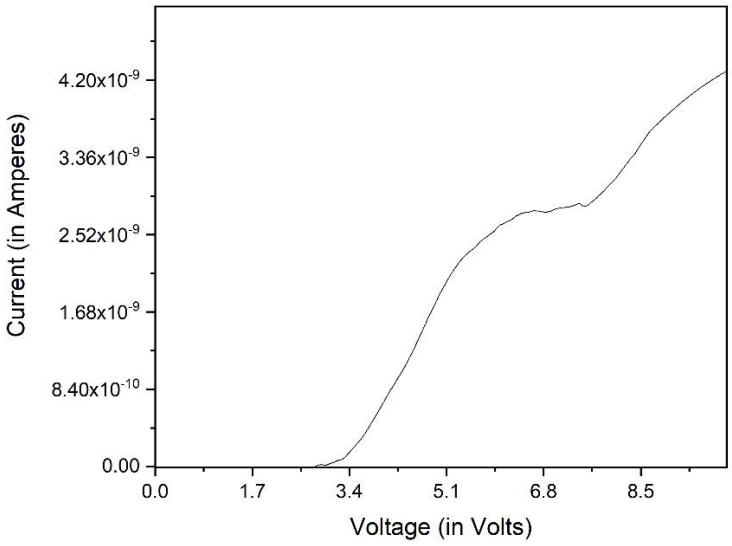


Figure 3.14(b): IV Characteristics of Two Terminal ZnO NW-based Device under 5V Bias Voltage

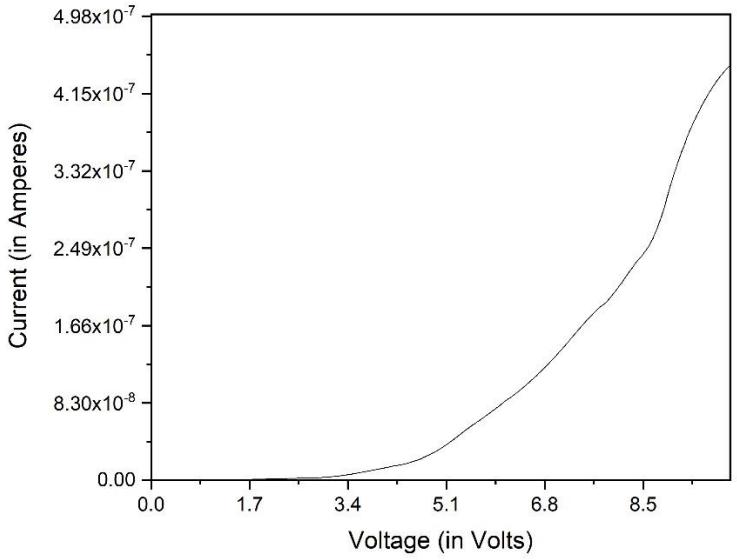


Figure 3.14(c): IV Characteristics of Two Terminal ZnO NW-based Device under 7.5V Bias Voltage

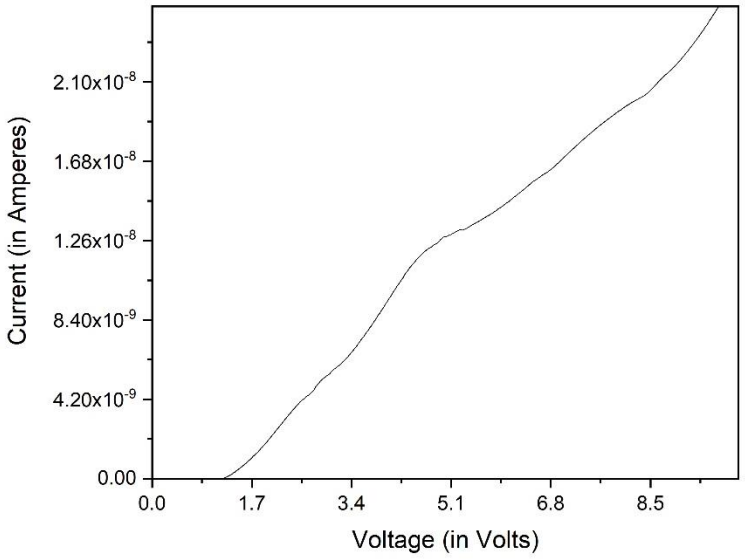


Figure 3.14(d): IV Characteristics of Two Terminal ZnO NW-based Device under 10V Bias Voltage

For Two Terminal ZnO NW-based Device under different Bias Voltages non-linear IV Characteristics are observed. The reason for non-linear IV Characteristics can be explained as follows-

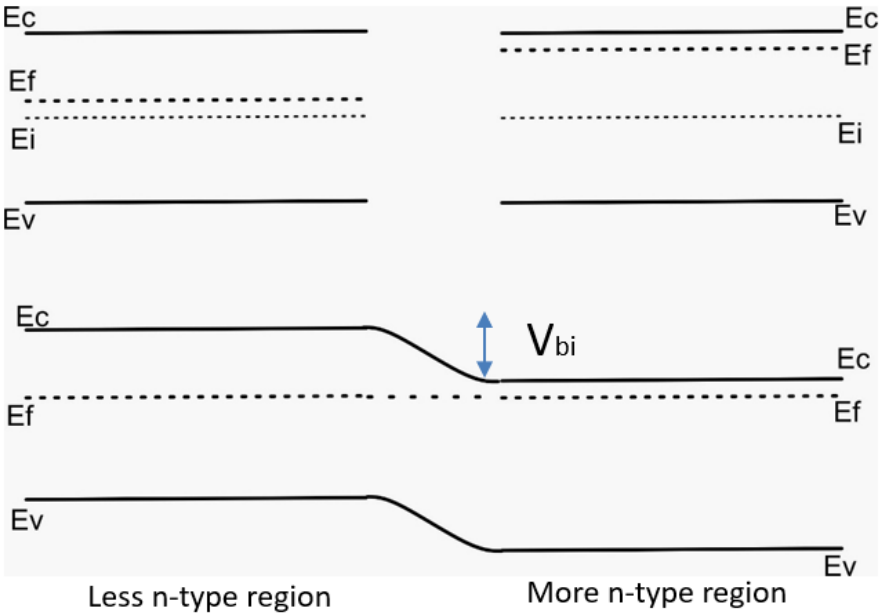


Figure 3.15: Probable Energy Band Diagram observed in Two Terminal ZnO NW-based Device

From Band Diagram point of view, it can be observed that the Less n-type Region has less electron affinity and the More n-type Region has more electron affinity. Subsequently, the Fermi Level for More n-type Region will be more closer to the Conduction Band Minima compared to the Fermi Level for Less n-type Region. When two Regions with different electron affinities come into contact, their energy bands may align in such a way that an energy barrier is formed at the interface which is often termed as "Built-in Potential". This Built-in-Potential (V_{bi}) acts as a barrier which opposes the flow of charge carriers (electrons or holes), resulting in Non-Linear IV Characteristics.

- **I-V Characteristics observed in Three Terminal Device**

After connecting the third terminal to the device, further experiments are performed. The voltage applied in the third terminal acts as the Gate Voltage to the device and the three terminal device that has been developed can be termed as Gated Voltage Assisted ZnO Nanowire based n-n^+ heterostructure device. By varying the Gate Voltage (V_{gs}) different I_d vs V_{ds} curves are obtained for all the devices. Figure 3.16 (a)-(d) demonstrates all those I_d vs V_{ds} characteristics curves.

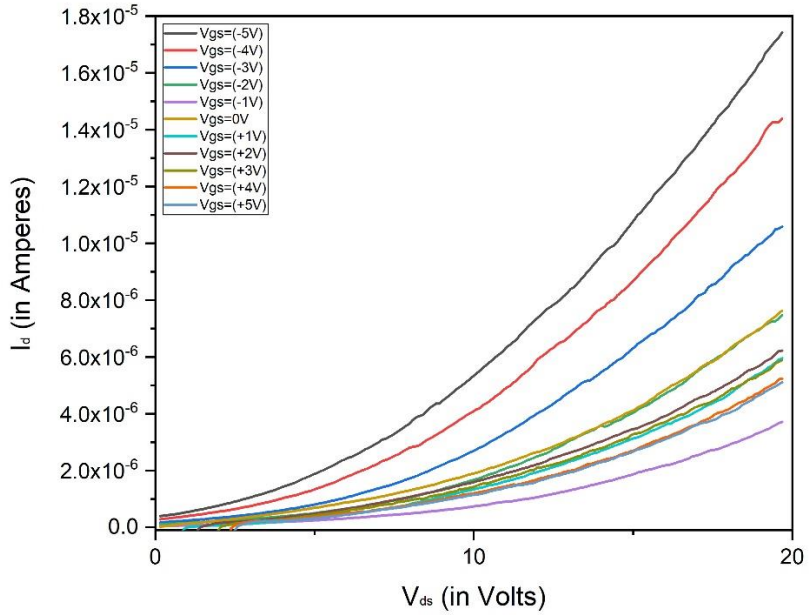


Figure 3.16(a): I_d vs V_{ds} Curve for Three Terminal ZnO NW-based Device under 2.5V Bias Voltage (under ambient condition)

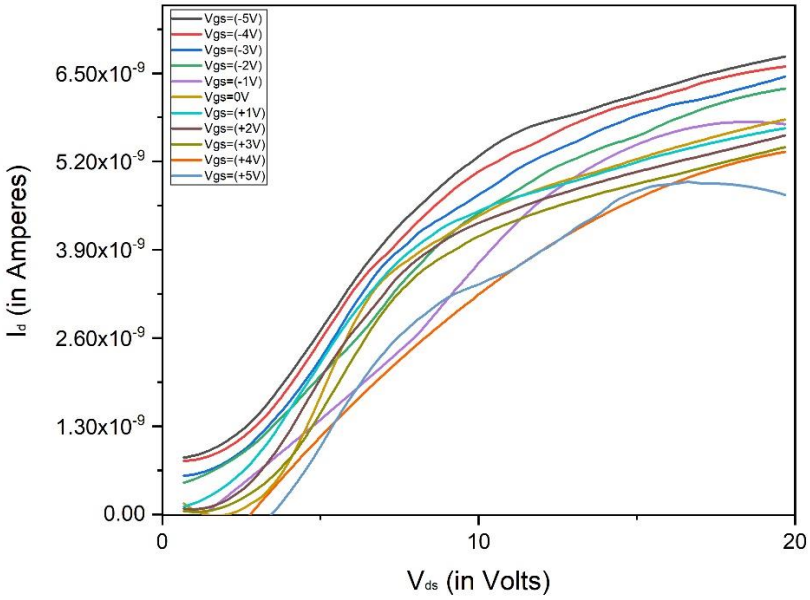


Figure 3.16(b): I_d vs V_{ds} Curve for Three Terminal ZnO NW-based Device under 5V Bias Voltage (under ambient condition)

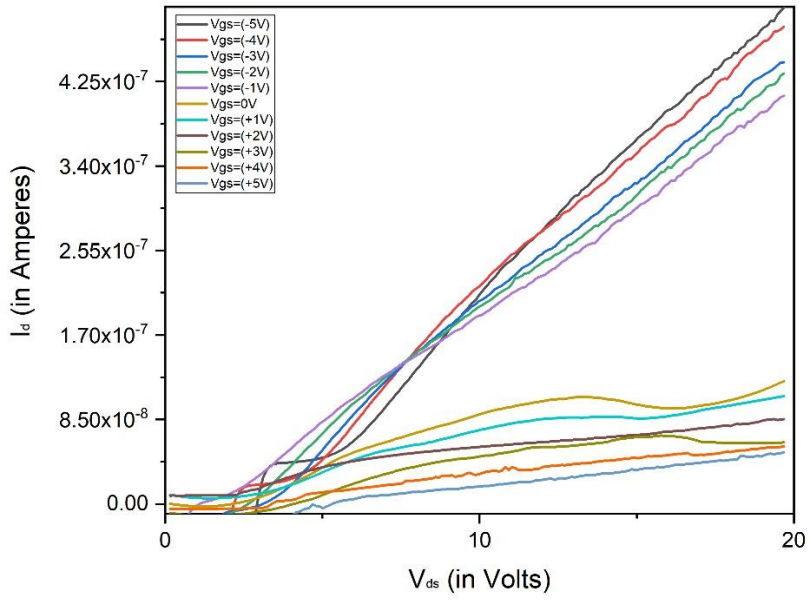


Figure 3.16(c): I_d vs V_{ds} Curve for Three Terminal ZnO NW-based Device under 7.5V Bias Voltage (under ambient condition)

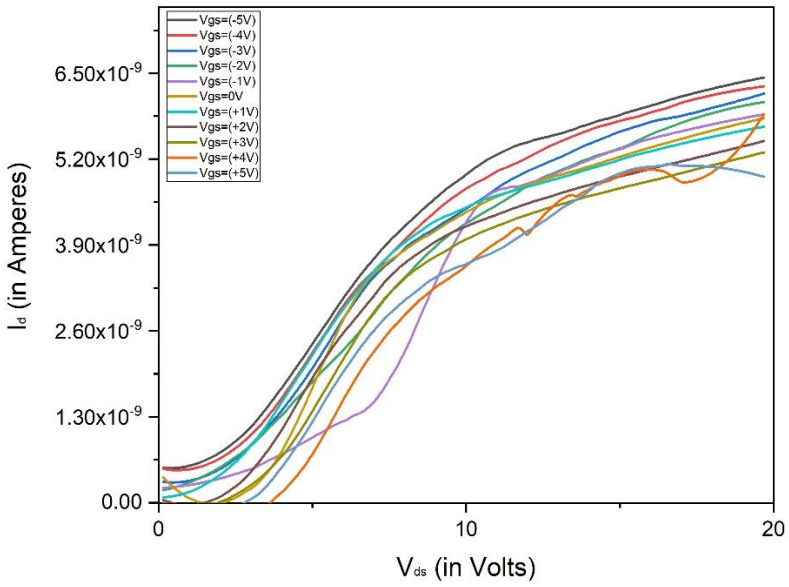


Figure 3.16(d): I_d vs V_{ds} Curve for Three Terminal ZnO NW-based Device under 10V Bias Voltage (under ambient condition)

From all the above I_d vs V_{ds} Curves it has been observed that - by increasing the Gate-to-Source Voltage (V_{gs}) from (-5)V to (+5)V the Drain Current (I_d) gradually decreases with respect to Drain-to-Source Voltage (V_{ds}). The probable reason for that can be explained as follows-

The device that has been fabricated has two regions- one is More n-type Region, where the number of negatively charged electrons is more and the other one is Less n-type Region where the number of negatively charged electrons is comparatively less. In between these two regions a junction is formed. This junction region is depleted of mobile charge carriers, that's why it can be called as Depletion Region. The Gate-to-Source Voltage (V_{gs}) terminal is connected to this Depletion Region.

On applying positive Gate-to-Source Voltage (V_{gs}) the negatively charged electrons are getting attracted towards the terminal where V_{gs} is applied. So, Depletion Width increases and Channel Width decreases. On increasing the positive V_{gs} more number of electrons are

getting accumulated towards the terminal where V_{gs} is applied. As a result, Depletion Width further increases and Channel width further decreases. This restricts the flow of charge carriers. Hence, Drain Current (I_d) gradually decreases upon increasing positive Gate-to-Source Voltage (V_{gs}).

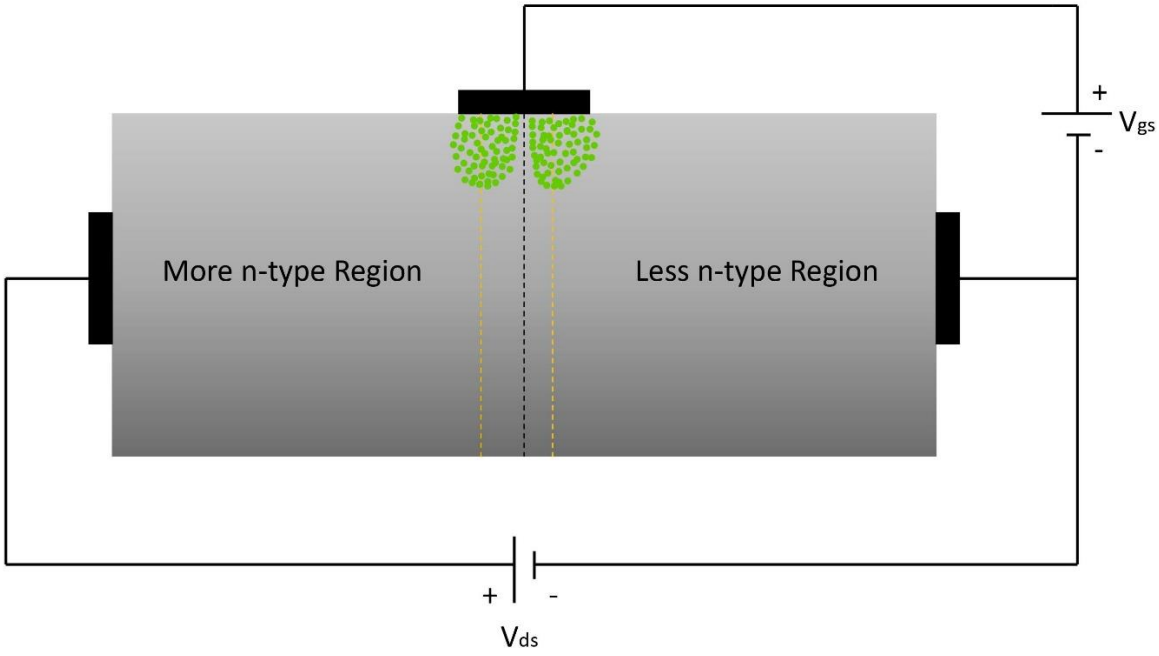


Figure 3.17(a): Schematic Diagram of the Device under positive Gate-to-Source Voltage (V_{gs})

On applying negative Gate-to-Source Voltage (V_{gs}) the negatively charged electrons are getting pulled away from the terminal where V_{gs} is applied. So, Depletion Width decreases and Channel Width increases. On increasing the negative V_{gs} more number of electrons are getting pulled away from the terminal where V_{gs} is applied. As a result, Depletion Width further decreases and Channel Width further increases. This helps the flow of charge carriers. Hence, Drain Current (I_d) gradually increases upon increasing negative Gate-to-Source Voltage (V_{gs}).

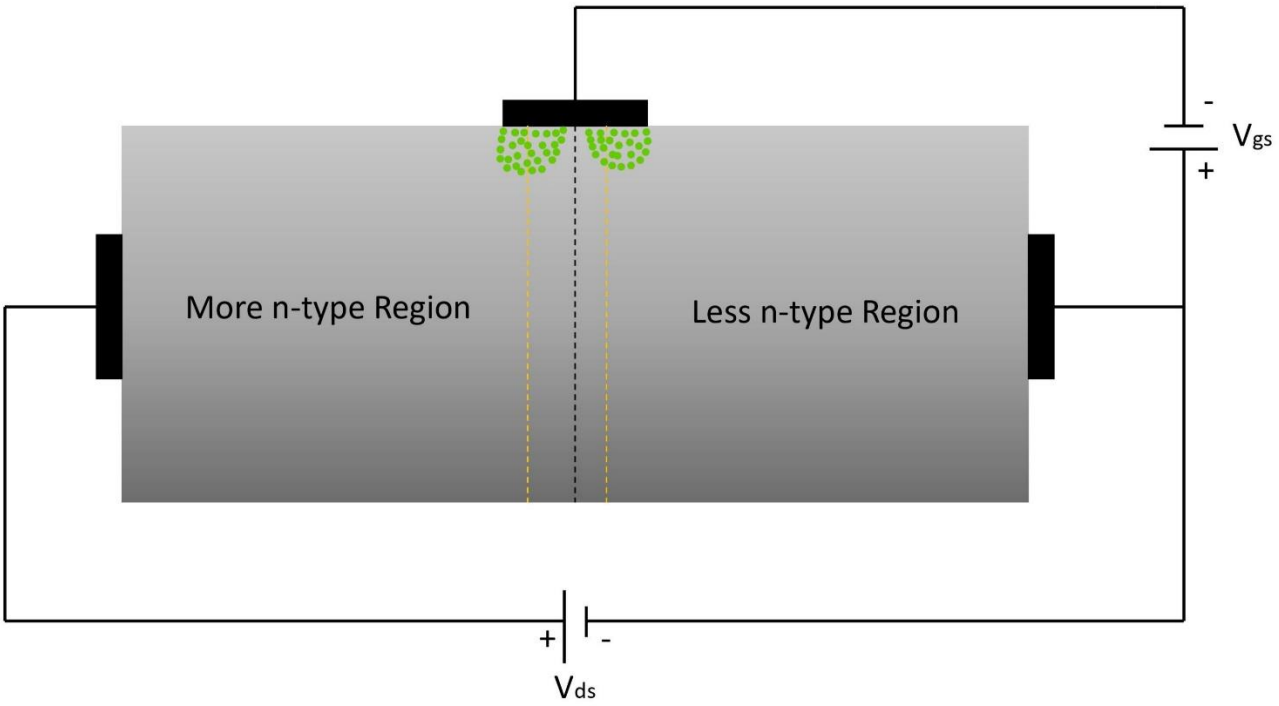


Figure 3.17(b): Schematic Diagram of the Device under negative Gate-to-Source Voltage (V_{gs})

REFERENCES:

1. McPeak, K.M.; Le, T.P.; Britton, N.G.; Nickolov, Z.S.; Elabd, Y.A.; Baxter, J.B. Chemical Bath Deposition of ZnO Nanowires at Near-Neutral pH Conditions without Hexamethylenetetramine (HMTA): Understanding the Role of HMTA in ZnO Nanowire Growth. ACS Publications, Langmuir 2011, 27, 3672-3677.
2. Azmi, Z.H.; Aris, S.N.M.; Abubakar, S.; Sagadevan, S.; Siburian, R.; Paiman, S. Effect of Seed Layer on the Growth of Zinc Oxide Nanowires by Chemical Bath Deposition Method. Coatings 2022, 12, 474.
3. Parize, R.; Garnier, J.; Chaix-Pluchery, O.; Verrier, C.; Appert, E.; Consonni, V. Effects of Hexamethylenetetramine on the Nucleation and Radial Growth of ZnO Nanowires by Chemical Bath Deposition. ACS Publications, J. Phys. Chem. C 2016, 120, 5242-5250.
4. Paul, S.; Das, A.; Chakraborty, A.; Chakraborty, B.; Palit, M.; Chattopadhyay, D.; Chattopadhyay, S. Growth and characterization of high quality ZnO nanowires by novel CBD/CBD technique. Elsevier Publications 2014, Proceedings of 1st International Science & Technology Congress 2014, 467-471.
5. Bhattacharya, S.; Saha, R.; Sikdar, S.; Mandal, S.; Das, C.; Chattopadhyay, S. Investigation of density and alignment of ZnO- nanowires grown by double-step chemical bath deposition (CBD/CBD) technique on metallic, insulating and semiconducting substrates. IEEE 2020.
6. Paul, S.; Das, A.; Palit, M.; Bhunia, S.; Karmakar, A.; Chattopadhyay, C. Investigation of the properties of single-step and double-step grown ZnO nanowires using chemical bath deposition technique. Adv. Mater. Lett. 2016, 7(8), 610-615.

7. Bhattacharya, S.; Saha, R.; Mandal, S.; Bhattacharya, D.; Chattopadhyay, S. Voltage-assisted selective growth of ZnO nanowires on metal/semiconductor surfaces employing hydrothermal double-step CBD/CBD growth technique. J Mater Sci: Mater Electron, 2023, 34, 2319.
8. Dey, S.; Nag, S.; Santra, S.; Ray, S.K.; Guha, P.K. Voltage-controlled NiO/ZnO p–n heterojunction diode: a new approach towards selective VOC sensing. Nature, Microsystems & Nanoengineering, 2020, 6, 35.
9. Nag, S.; Dey, S.; Das, D.; Guha, P.K. Adsorption Mediated n-Type ZnO Surface Reconstruction for Optically Enhanced Volatile Organic Compound Sensing. *ACS Applied Electronic Materials* **2022** *4* (8), 3825-3833.

CHAPTER 4

4. Heavy Metal Ion Sensing by Gated Voltage Assisted Zinc Oxide Nanowire-based n-n^+ Heterostructure Device

Heavy Metal Ions are chemical ions with a specific gravity at least five times than that of water. Certain heavy metals are nutritionally essential for a healthy human body. If heavy metals are consumed above a certain permissible concentration then that can be lethal. Hence, heavy metal ion detection is necessary.

Heavy metal sensing experiments were performed to further investigate the properties and sensing capabilities of the Gated Voltage Assisted Zinc Oxide Nanowire-based n-n^+ Heterostructure Device.

To study the selectivity of the fabricated sensing devices, these were exposed to similar concentrations of different heavy metal ions [e.g. 100ppm Cr(VI), 100ppm Cu(II), 100ppm Fe(II), 100ppm Ni(III)]. For sensing the fabricated devices were operated in Probe Station shown in Figure 3.11 of Chapter 3.

The Response of the sensing devices can be expressed in percentage by the following relation:

$$\text{Response } \% = \left(\frac{Isense - Io}{Io} X\ 100\right) \%$$

where, Io = bare device current

$Isense$ = device current in the presence of analyte



Figure 4.1: Different Heavy Metal Ions used for sensing purpose

4.1 Results and Discussions

4.1.1 Sensing using Three Terminal ZnO NW-based Device under 2.5V Bias Voltage

Figure 4.2 (a)-(d) demonstrates the I_d vs V_{ds} Curves obtained in Three Terminal ZnO NW-based Device under 2.5V Bias Voltage upon exposure to different heavy metal ions of similar concentrations.

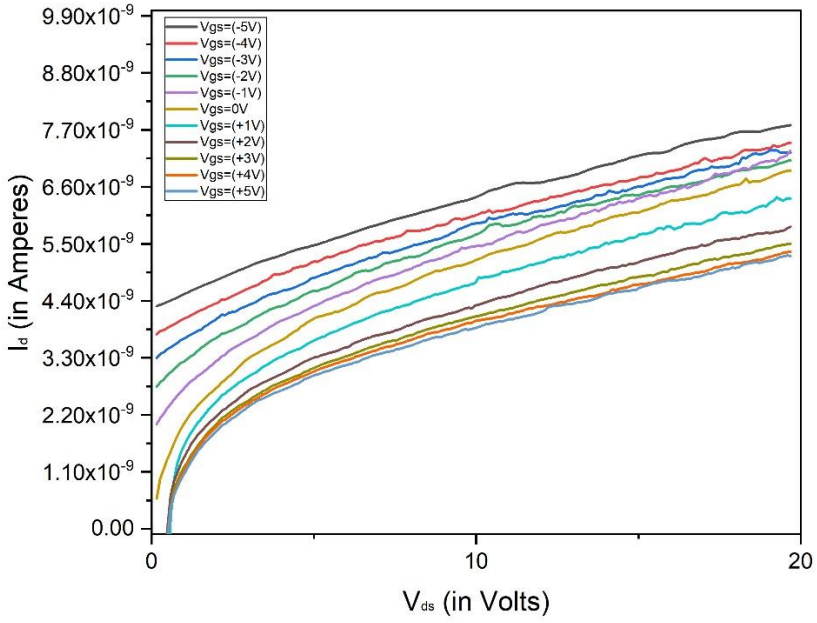


Figure 4.2(a): I_d vs V_{ds} Curve for Three Terminal ZnO NW-based Device under 2.5V Bias Voltage [exposed to 100ppm Cr(VI)]

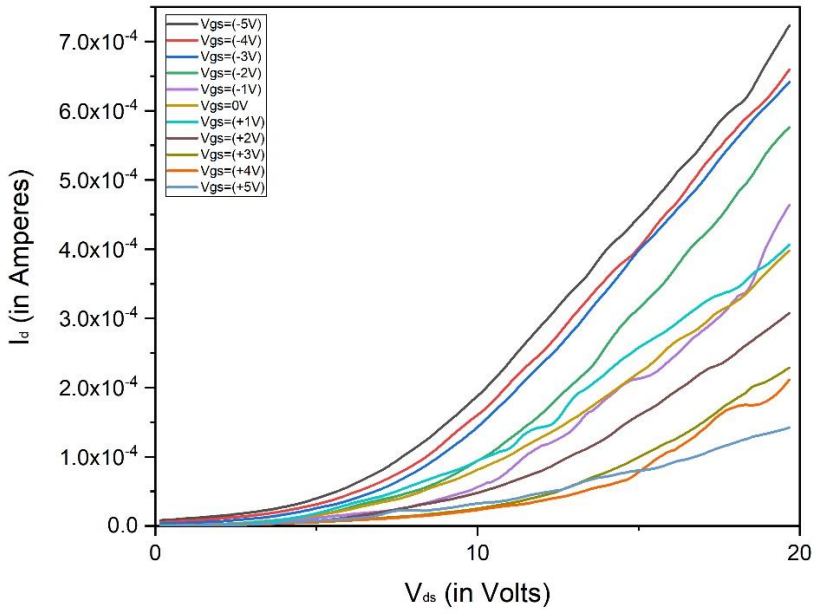


Figure 4.2(b): I_d vs V_{ds} Curve for Three Terminal ZnO NW-based Device under 2.5V Bias Voltage [exposed to 100ppm Cu(II)]

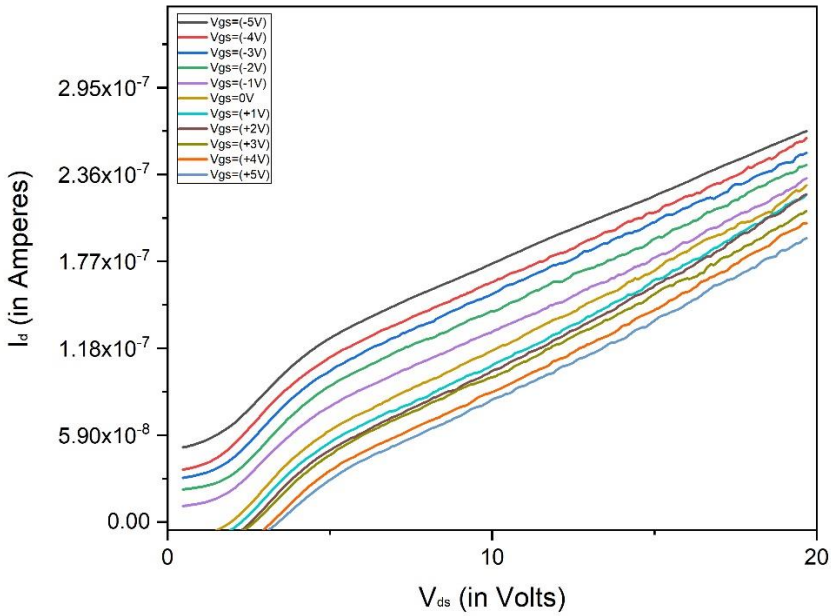


Figure 4.2(c): I_d vs V_{ds} Curve for Three Terminal ZnO NW-based Device under 2.5V Bias Voltage [exposed to 100ppm Fe(II)]

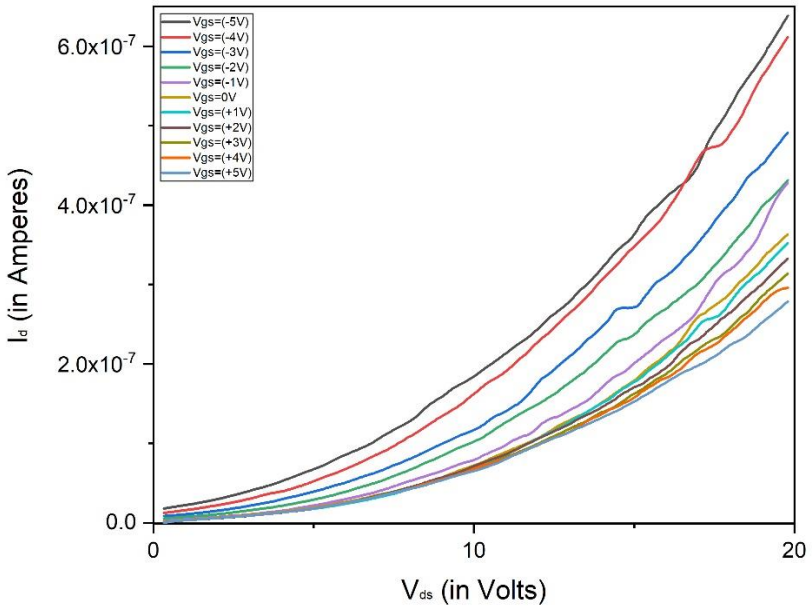


Figure 4.2(d): I_d vs V_{ds} Curve for Three Terminal ZnO NW-based Device under 2.5V Bias Voltage [exposed to 100ppm Ni(III)]

The Response of the Three Terminal ZnO NW-based Device under 2.5V Bias Voltage for different analytes are shown in Table 4.1.

Table 4.1: Response of Three Terminal ZnO NW-based Device under 2.5V Bias Voltage

Device	Gate to Source Voltage (Vgs)	Measured Analyte	Response in %
Three Terminal ZnO NW-based Device under 2.5V Bias Voltage	(-5V)	100ppm Cr	99.96
		100ppm Cu	97.54
		100ppm Fe	76.20
		100ppm Ni	96.35
	(-4V)	100ppm Cr	99.95
		100ppm Cu	97.77
		100ppm Fe	75.4
		100ppm Ni	95.89
	(-3V)	100ppm Cr	99.93
		100ppm Cu	98.39
		100ppm Fe	64.07
		100ppm Ni	95.35
	(-2V)	100ppm Cr	99.91
		100ppm Cu	98.73
		100ppm Fe	36.19
		100ppm Ni	94.19
	(-1V)	100ppm Cr	99.81
		100ppm Cu	99.18
		100ppm Fe	21.45
		100ppm Ni	88.63
	0V	100ppm Cr	99.91
		100ppm Cu	98.10
		100ppm Fe	65.02
		100ppm Ni	95.30
	(+1V)	100ppm Cr	99.89
		100ppm Cu	98.63
		100ppm Fe	21.37
		100ppm Ni	93.97
	(+2V)	100ppm Cr	99.91
		100ppm Cu	97.96
		100ppm Fe	57.85
		100ppm Ni	94.68
	(+3V)	100ppm Cr	99.91
		100ppm Cu	97.86
		100ppm Fe	16.42
		100ppm Ni	94.85
	(+4V)	100ppm Cr	99.91
		100ppm Cu	97.42
		100ppm Fe	0.00
		100ppm Ni	94.35
	(+5V)	100ppm Cr	99.91
		100ppm Cu	96.42
		100ppm Fe	10.24
		100ppm Ni	94.71

The Response vs Analyte Curves of Three Terminal ZnO NW-based Device under 2.5V Bias Voltage are shown below-

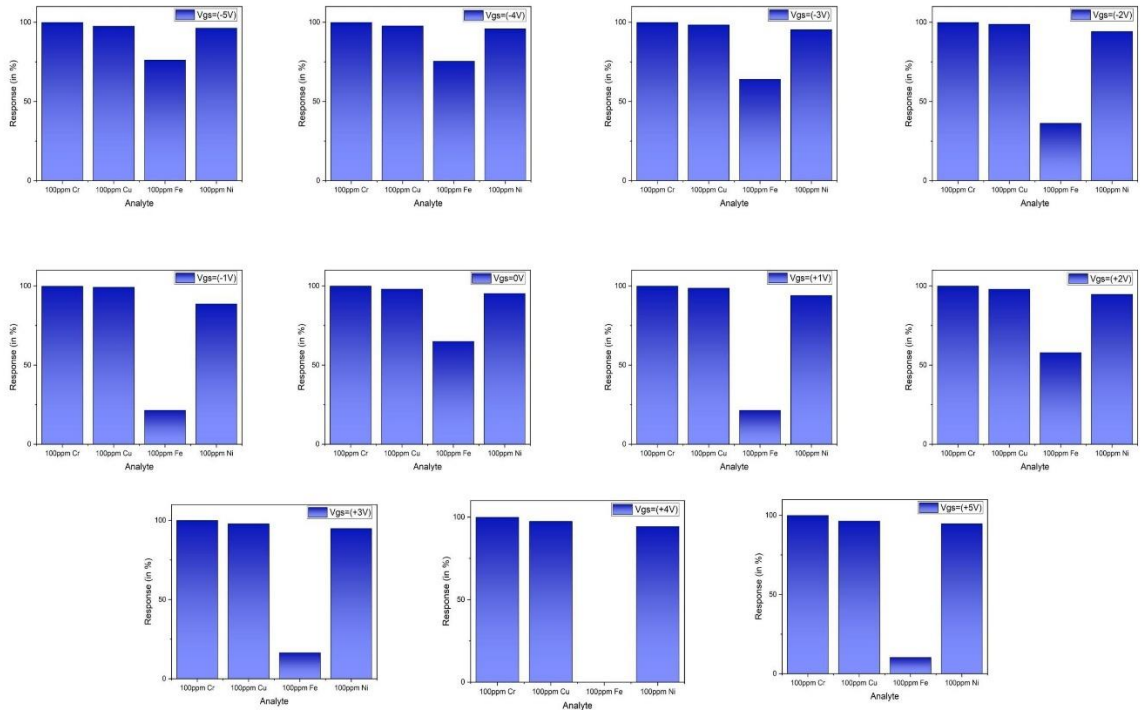


Figure 4.3: Response vs Analyte Curves of Three Terminal ZnO NW-based Device under 2.5V Bias Voltage [V_{gs} varies from (-5)V to (+5)V]

4.1.2 Sensing using Three Terminal ZnO NW-based Device under 5V Bias Voltage

Figure 4.4 (a)-(d) demonstrates the I_d vs V_{ds} Curves obtained in Three Terminal ZnO NW-based Device under 5V Bias Voltage upon exposure to different heavy metal ions of similar concentrations.

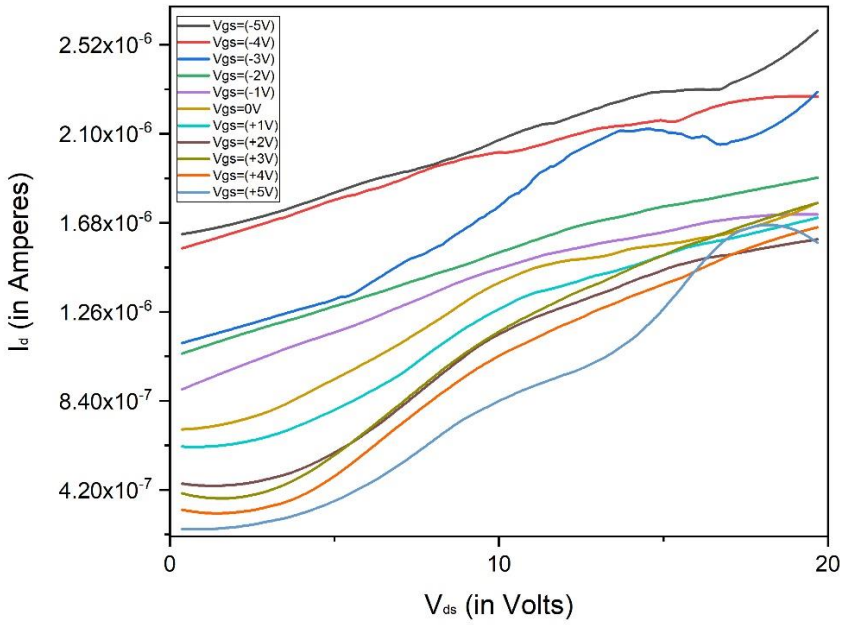


Figure 4.4(a): I_d vs V_{ds} Curve for Three Terminal ZnO NW-based Device under 5V Bias Voltage [exposed to 100ppm Cr(VI)]

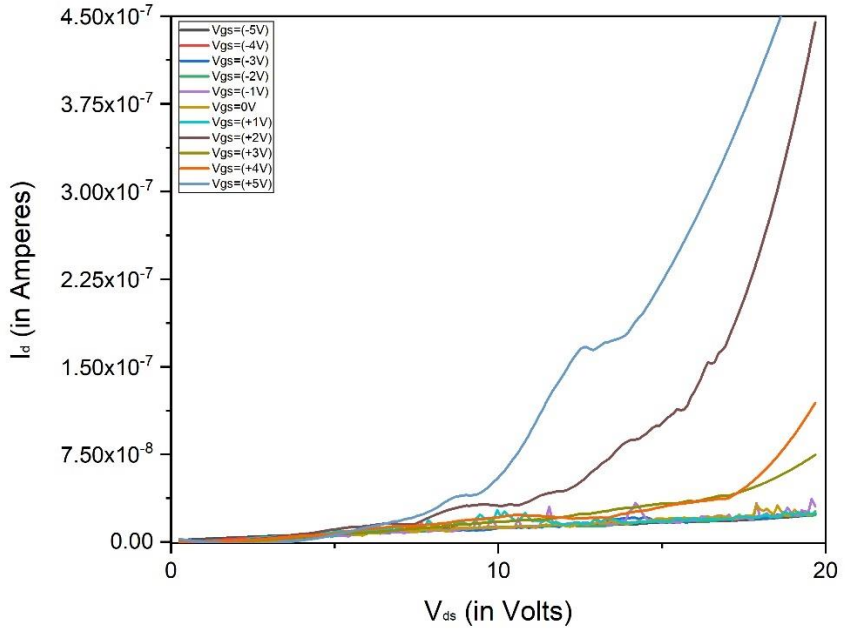


Figure 4.4(b): I_d vs V_{ds} Curve for Three Terminal ZnO NW-based Device under 5V Bias Voltage [exposed to 100ppm Cu(II)]

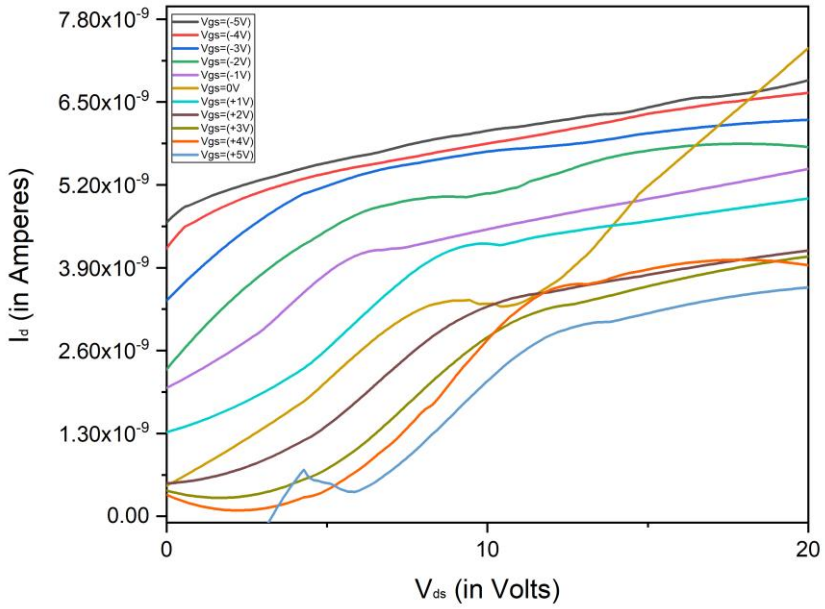


Figure 4.4(c): I_d vs V_{ds} Curve for Three Terminal ZnO NW-based Device under 5V Bias Voltage [exposed to 100ppm Fe(II)]

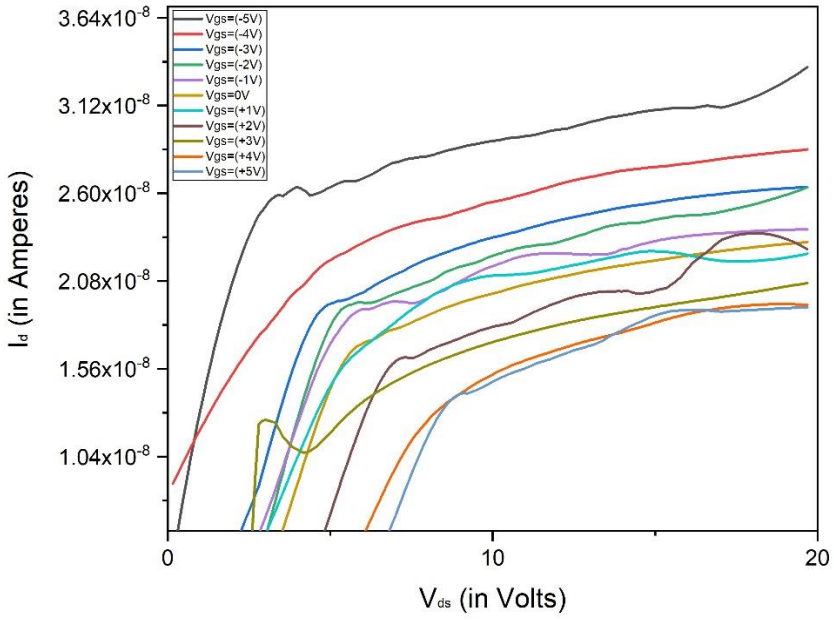


Figure 4.4(d): I_d vs V_{ds} Curve for Three Terminal ZnO NW-based Device under 5V Bias Voltage [exposed to 100ppm Ni(III)]

The Response of the Three Terminal ZnO NW-based Device under 5V Bias Voltage for different analytes are shown in Table 4.2.

Table 4.2: Response of Three Terminal ZnO NW-based Device under 5V Bias Voltage

Device	Gate to Source Voltage (Vgs)	Measured Analyte	Response in %
Three Terminal ZnO NW-based Device under 5V Bias Voltage	(-5V)	100ppm Cr	99.66
		100ppm Cu	84.82
		100ppm Fe	16.34
		100ppm Ni	89.91
	(-4V)	100ppm Cr	99.63
		100ppm Cu	87.53
		100ppm Fe	14.18
		100ppm Ni	88.40
	(-3V)	100ppm Cr	99.67
		100ppm Cu	81.85
		100ppm Fe	13.40
		100ppm Ni	84.16
	(-2V)	100ppm Cr	99.64
		100ppm Cu	85.18
		100ppm Fe	9.12
		100ppm Ni	87.20
	(-1V)	100ppm Cr	99.62
		100ppm Cu	92.36
		100ppm Fe	4.79
		100ppm Ni	86.80
	0V	100ppm Cr	99.70
		100ppm Cu	87.67
		100ppm Fe	47.52
		100ppm Ni	86.34
	(+1V)	100ppm Cr	67.41
		100ppm Cu	99.24
		100ppm Fe	99.89
		100ppm Ni	99.30
	(+2V)	100ppm Cr	99.73
		100ppm Cu	98.90
		100ppm Fe	11.08
		100ppm Ni	85.80
	(+3V)	100ppm Cr	99.76
		100ppm Cu	95.39
		100ppm Fe	8.97
		100ppm Ni	83.89
	(+4V)	100ppm Cr	99.76
		100ppm Cu	96.46
		100ppm Fe	17.35
		100ppm Ni	83.47

	(+5V)	100ppm Cr	99.75
		100ppm Cu	99.64
		100ppm Fe	5.51
		100ppm Ni	83.28

The Response vs Analyte Curves of Three Terminal ZnO NW-based Device under 5V Bias Voltage are shown below-

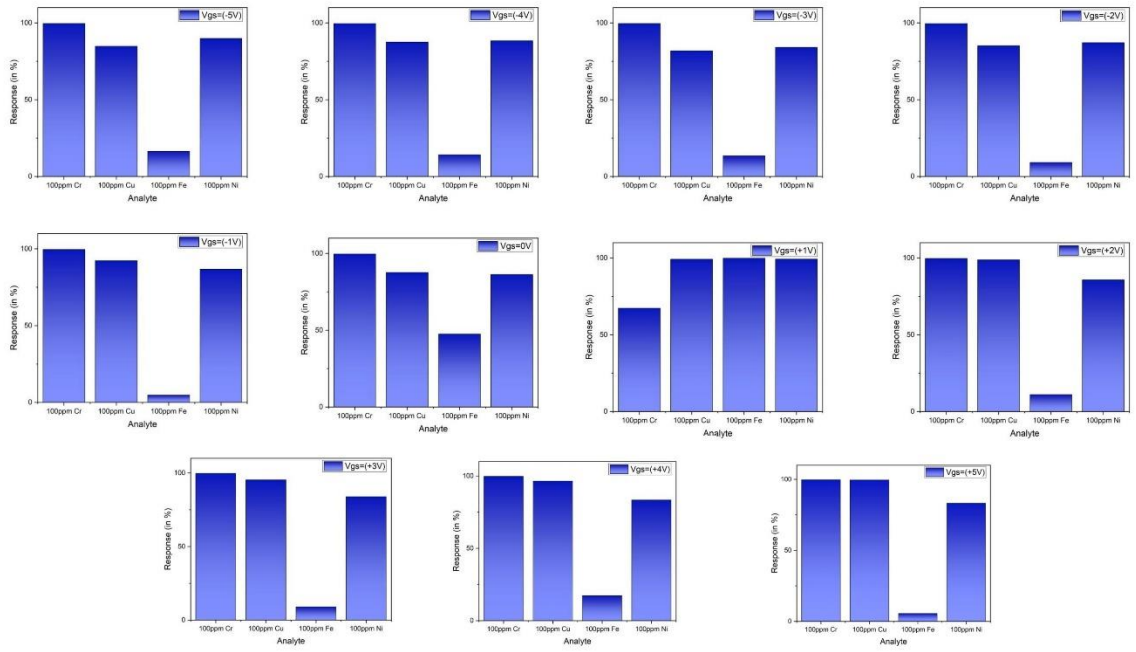


Figure 4.5: Response vs Analyte Curves of Three Terminal ZnO NW-based Device under 5V Bias Voltage [V_{gs} varies from (-5)V to (+5)V]

4.1.3 Sensing using Three Terminal ZnO NW-based Device under 7.5V Bias Voltage

Figure 4.6 (a)-(d) demonstrates the I_d vs V_{ds} Curves obtained in Three Terminal ZnO NW-based Device under 7.5V Bias Voltage upon exposure to different heavy metal ions of similar concentrations.

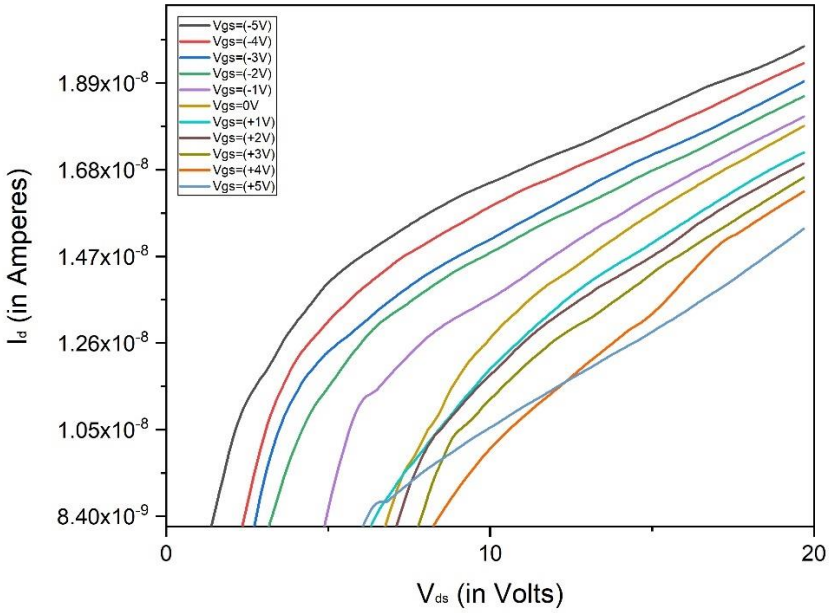


Figure 4.6(a): I_d vs V_{ds} Curve for Three Terminal ZnO NW-based Device under 7.5V Bias Voltage [exposed to 100ppm Cr(VI)]

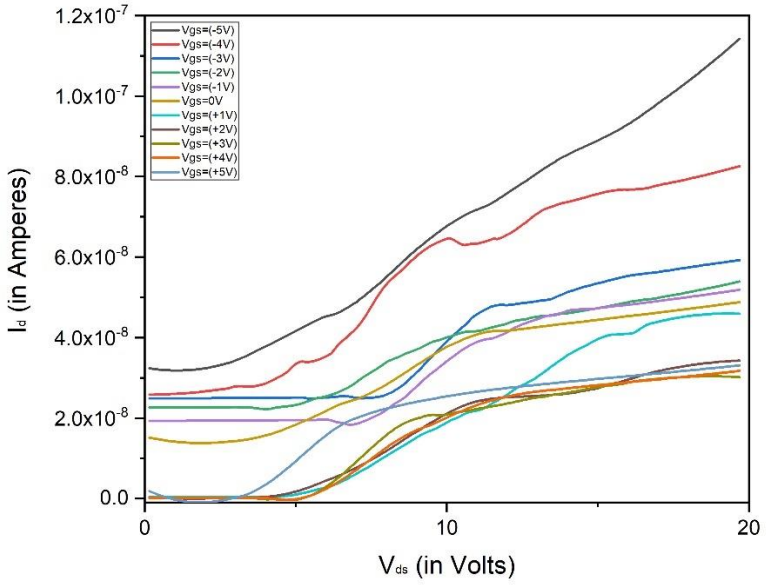


Figure 4.6(b): I_d vs V_{ds} Curve for Three Terminal ZnO NW-based Device under 7.5V Bias Voltage [exposed to 100ppm Cu(II)]

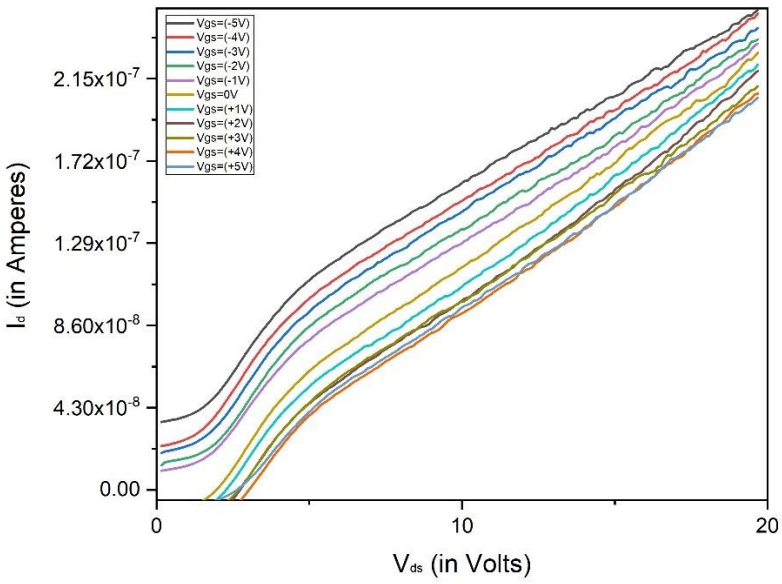


Figure 4.6(c): I_d vs V_{ds} Curve for Three Terminal ZnO NW-based Device under 7.5V Bias Voltage [exposed to 100ppm Fe(II)]

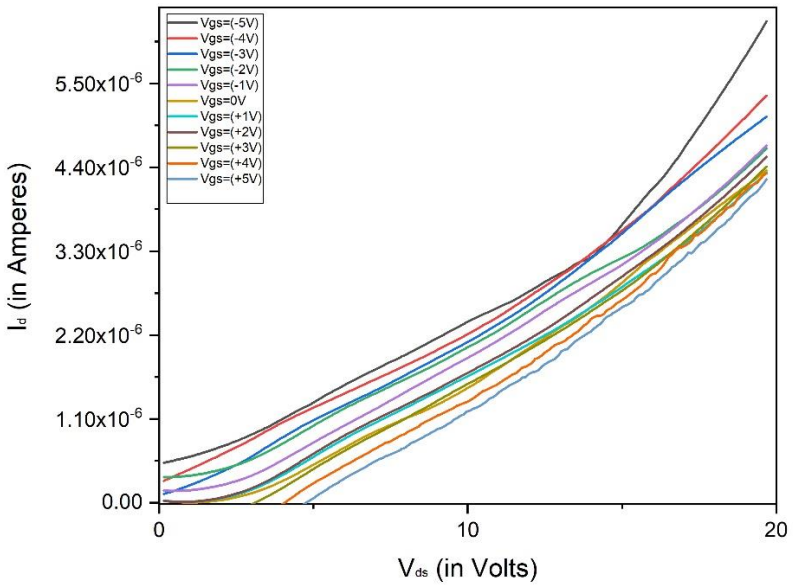


Figure 4.6(d): I_d vs V_{ds} Curve for Three Terminal ZnO NW-based Device under 7.5V Bias Voltage [exposed to 100ppm Ni(III)]

The Response of the Three Terminal ZnO NW-based Device under 7.5V Bias Voltage for different analytes are shown in Table 4.3.

Table 4.3: Response of Three Terminal ZnO NW-based Device under 7.5V Bias Voltage

Device	Gate to Source Voltage (Vgs)	Measured Analyte	Response in %
Three Terminal ZnO NW-based Device under 7.5V Bias Voltage	(-5V)	100ppm Cr	70.65
		100ppm Cu	23.75
		100ppm Fe	68.90
		100ppm Ni	98.79
	(-4V)	100ppm Cr	69.57
		100ppm Cu	11.49
		100ppm Fe	72.00
		100ppm Ni	98.78

	(-3V)	100ppm Cr	76.16
		100ppm Cu	55.33
		100ppm Fe	64.89
		100ppm Ni	98.46
	(-2V)	100ppm Cr	76.24
		100ppm Cu	60.36
		100ppm Fe	64.71
		100ppm Ni	98.27
	(-1V)	100ppm Cr	81.70
		100ppm Cu	67.10
		100ppm Fe	56.14
		100ppm Ni	97.84
	0V	100ppm Cr	85.17
		100ppm Cu	69.91
		100ppm Fe	52.46
		100ppm Ni	97.34
	(+1V)	100ppm Cr	95.87
		100ppm Cu	88.35
		100ppm Fe	73.14
		100ppm Ni	90.65
	(+2V)	100ppm Cr	96.30
		100ppm Cu	92.62
		100ppm Fe	88.16
		100ppm Ni	90.13
	(+3V)	100ppm Cr	96.38
		100ppm Cu	93.32
		100ppm Fe	50.00
		100ppm Ni	90.19
	(+4V)	100ppm Cr	96.53
		100ppm Cu	93.26
		100ppm Fe	50.42
		100ppm Ni	90.37
	(+5V)	100ppm Cr	96.67
		100ppm Cu	92.24
		100ppm Fe	53.18
		100ppm Ni	90.54

The Response vs Analyte Curves of Three Terminal ZnO NW-based Device under 7.5V Bias Voltage are shown below-

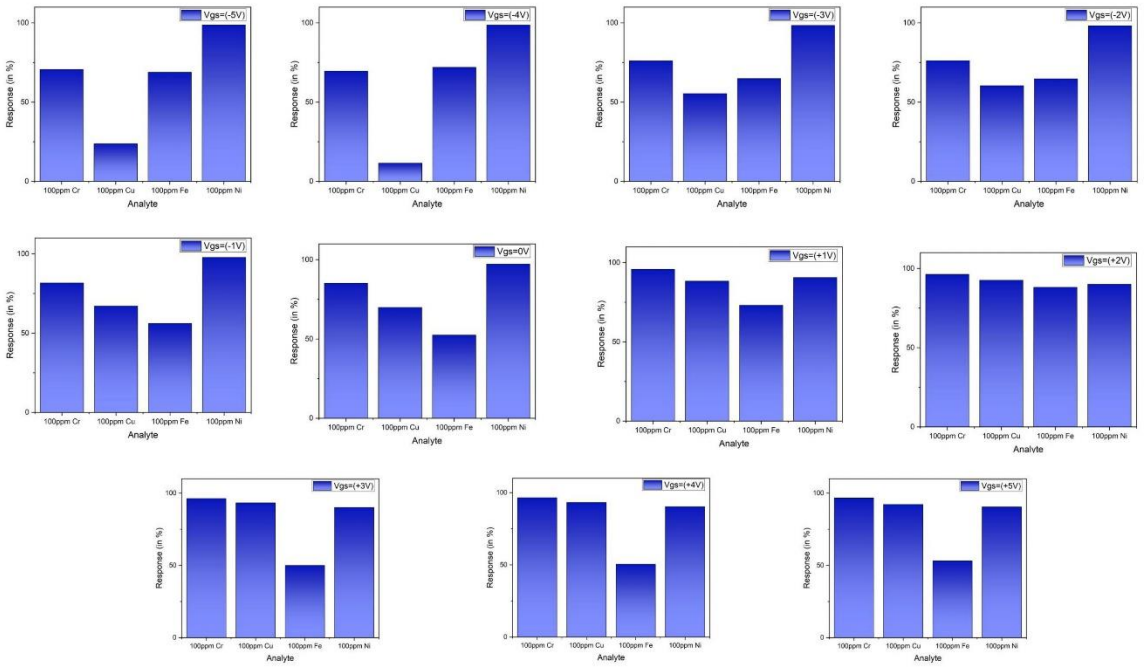


Figure 4.7: Response vs Analyte Curves of Three Terminal ZnO NW-based Device under 7.5V Bias Voltage [V_{gs} varies from (-5)V to (+5)V]

4.1.4 Sensing using Three Terminal ZnO NW-based Device under 10V Bias Voltage

Figure 4.8 (a)-(d) demonstrates the I_d vs V_{ds} Curves obtained in Three Terminal ZnO NW-based Device under 10V Bias Voltage upon exposure to different heavy metal ions of similar concentrations.

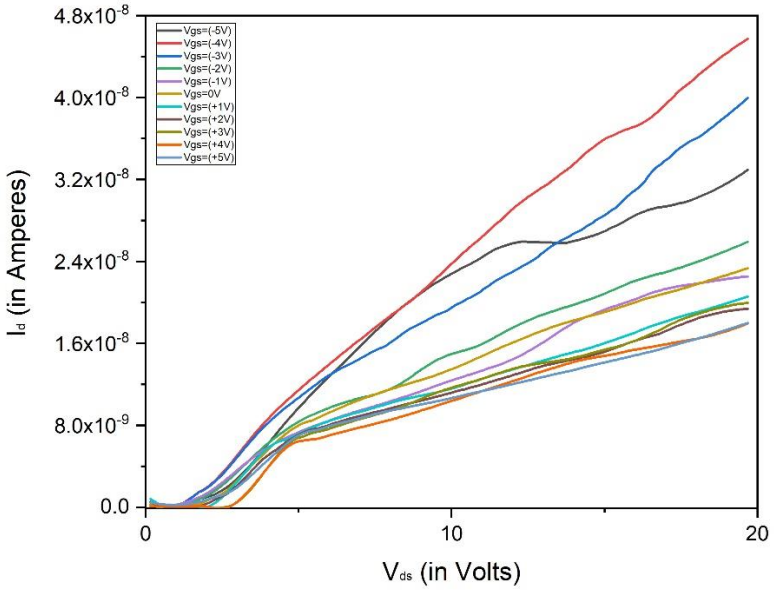


Figure 4.8(a): I_d vs V_{ds} Curve for Three Terminal ZnO NW-based Device under 10V Bias Voltage [exposed to 100ppm Cr(VI)]

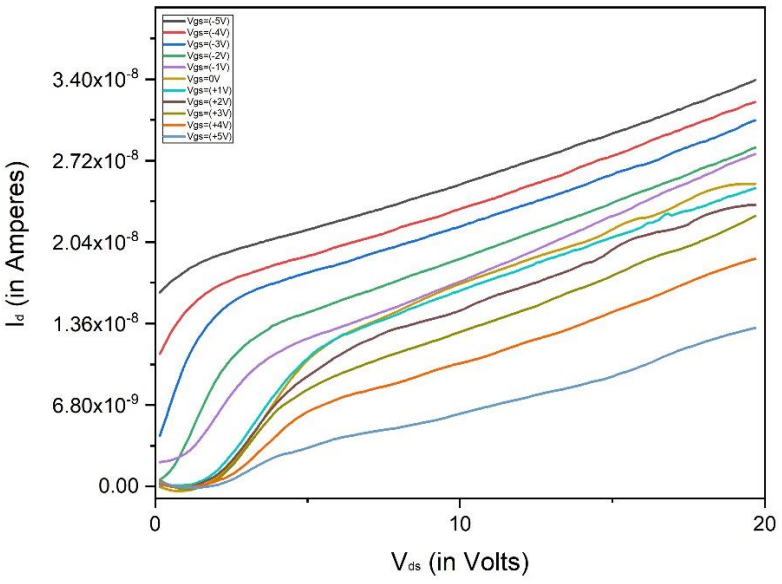


Figure 4.8(b): I_d vs V_{ds} Curve for Three Terminal ZnO NW-based Device under 10V Bias Voltage [exposed to 100ppm Cu(II)]

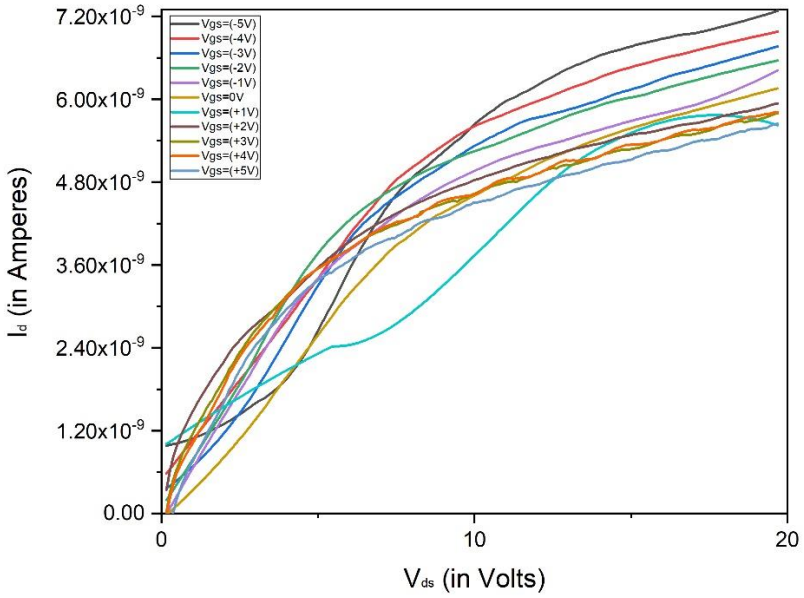


Figure 4.8(c): I_d vs V_{ds} Curve for Three Terminal ZnO NW-based Device under 10V Bias Voltage [exposed to 100ppm Fe(II)]

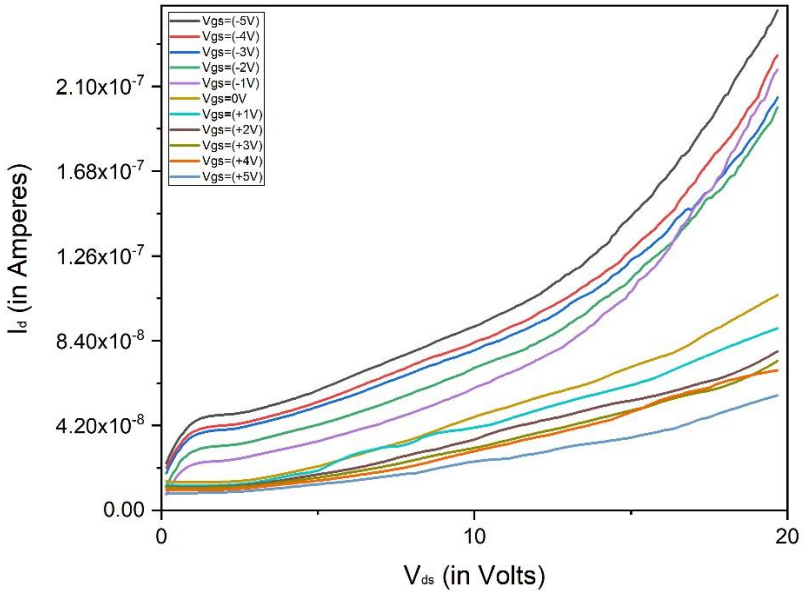


Figure 4.8(d): I_d vs V_{ds} Curve for Three Terminal ZnO NW-based Device under 10V Bias Voltage [exposed to 100ppm Ni(III)]

The Response of the Three Terminal ZnO NW-based Device under 10V Bias Voltage for different analytes are shown in Table 4.4.

Table 4.4: Response of Three Terminal ZnO NW-based Device under 10V Bias Voltage

Device	Gate to Source Voltage (Vgs)	Measured Analyte	Response in %
Three Terminal ZnO NW-based Device under 10V Bias Voltage	(-5V)	100ppm Cr	66.67
		100ppm Cu	82.16
		100ppm Fe	7.15
		100ppm Ni	97.08
	(-4V)	100ppm Cr	65.93
		100ppm Cu	80.86
		100ppm Fe	3.58
		100ppm Ni	96.77
	(-3V)	100ppm Cr	70.34
		100ppm Cu	80.42
		100ppm Fe	9.16
		100ppm Ni	96.50
	(-2V)	100ppm Cr	68.91
		100ppm Cu	79.09
		100ppm Fe	6.40
		100ppm Ni	96.59
	(-1V)	100ppm Cr	72.67
		100ppm Cu	78.09
		100ppm Fe	10.31
		100ppm Ni	97.16
	0V	100ppm Cr	75.38
		100ppm Cu	77.72
		100ppm Fe	6.09
		100ppm Ni	93.50
	(+1V)	100ppm Cr	75.33
		100ppm Cu	77.58
		100ppm Fe	4.82
		100ppm Ni	92.89
	(+2V)	100ppm Cr	79.25
		100ppm Cu	77.01
		100ppm Fe	0.36
		100ppm Ni	92.21
	(+3V)	100ppm Cr	87.08
		100ppm Cu	75.86
		100ppm Fe	3.86
		100ppm Ni	90.68

	(+4V)	100ppm Cr	87.88
		100ppm Cu	70.88
		100ppm Fe	2.59
		100ppm Ni	91.58
	(+5V)	100ppm Cr	84.10
		100ppm Cu	61.54
		100ppm Fe	11.51
		100ppm Ni	89.30

The Response vs Analyte Curves of Three Terminal ZnO NW-based Device under 10V Bias Voltage are shown below-

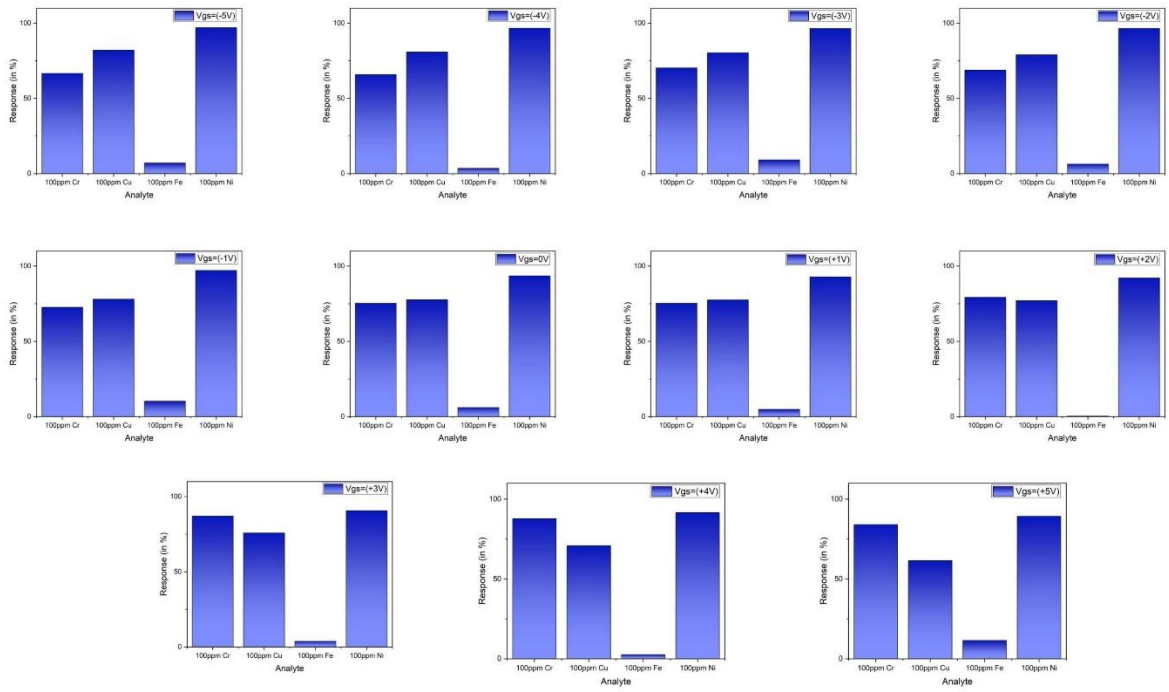


Figure 4.9: Response vs Analyte Curves of Three Terminal ZnO NW-based Device under 10V Bias Voltage [V_{gs} varies from (-5)V to (+5)V]

4.1.5 Mechanism of Heavy Metal Ion Sensing

Zinc Oxide is a n-type semiconductor in the nano regime due to the presence of surface oxygen vacancies. These vacancy sites act as adsorption sites for heavy metal ions. Actually these vacancy sites play the major role for sensing. On fabricating nanostructures with defects, the ease and surface area of adsorption was increased to a considerable extent leading to an efficient sensing performance.

On exposure of the Zinc Oxide Nanowire based sensing layer to different heavy metal ions, the cations are physisorbed on to the surface thereby depleting the surface electrons. Hence, the surface potential of the semiconductor changes. This results a change in current (*Isense*) in comparison to the current under ambient condition (*Io*).

4.2 Overall Response of the Devices and their Selectivity

The Response of the as-prepared devices for different heavy metal ions are shown in Figure 4.10.

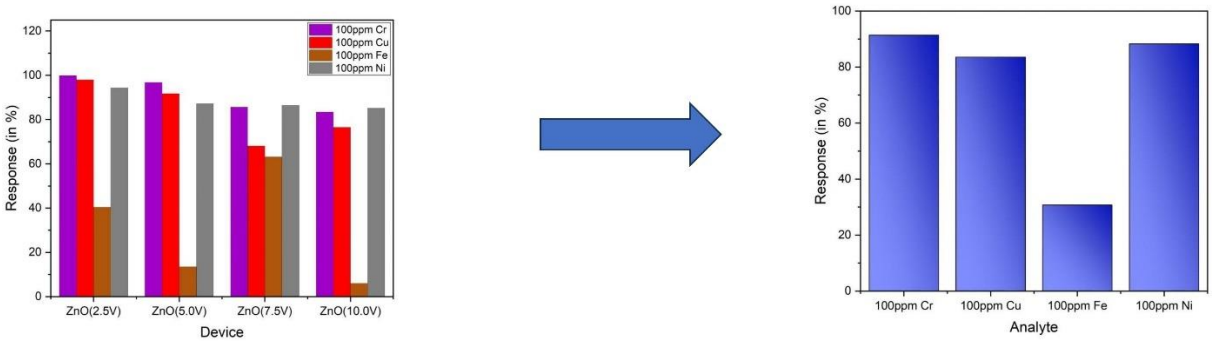


Figure 4.10: Overall Response Curves of the as-prepared Devices

Selectivity of a Sensing Device refers to its ability to recognize and measure a particular analyte without any interference. In short, Selectivity is the ability of a Sensing Device to identify a particular analyte in a mixed environment.

From the Overall Response Curves of the as-prepared Devices it can be concluded that the devices show responses towards Cr(VI), Cu(II) and Ni(III) ions, and not towards Fe(II) ions. Moreover, the Devices show highest response for Cr(VI) ions.

A Sensing Device is said to have good selectivity when its response towards a particular analyte is several times or even tens of times higher than the response towards other analytes. But, in these Devices the response towards a particular heavy metal ion is not several times higher than the responses towards other heavy metal ions. So, the as-prepared devices are not selective.

CHAPTER 5

5. Conclusion and Future Work

5.1 Conclusion

In conclusion, this thesis presented the fabrication and characterization of Gated Voltage Assisted Zinc Oxide Nanowire-based n-n^+ Heterostructure Devices under different Bias Voltages and their response towards the detection of several heavy metal ions namely Chromium(VI), Copper(II), Iron(II) & Nickel(III).

Zinc Oxide Nanowire-based Devices were fabricated by a Double Step Voltage Assisted Chemical Bath Deposition (CBD) Technique under different Bias Voltages i.e. 2.5V, 5.0V, 7.5V & 10V.

The synthesized materials were thoroughly characterized using XRD, FESEM & DRS. The particle size in different regions were determined using Scherrer Formula and Williamson-Hall Plot. The variation in Band Gap Energy in different regions was also observed from Diffuse Reflectance Spectroscopy (DRS) data, which indicates that the as-prepared devices are heterostructure devices.

Atfirst non-linear IV Characteristics Curves were obtained for two terminal devices. After that, a third terminal was connected (which acts as a Gate Terminal) and its corresponding I_d vs V_{ds} Characteristics Curves were studied under different Gate-to-Source Voltage (V_{gs}).

Finally, the Response & Selectivity of the as-prepared Gated Voltage Assisted Zinc Oxide Nanowire-based n-n^+ Heterostructure Devices towards different heavy metal ions are studied.

This thesis demonstrated the efficiency of Gated Voltage Assisted Zinc Oxide Nanowire-based n-n^+ Heterostructure Devices for the detection of Chromium(VI),

Copper(II), Iron(II) & Nickel(III) ions. The outcomes offer valuable insights into the development of novel sensing materials. This study lays the groundwork for future research endeavours in the field of heavy metal ion detection, environmental monitoring, and water safety.

5.2 Future Works

- Investigate the sensing response of the device towards other heavy metal ions.
- Further investigate the sensing performance of the device towards all the heavy metal ions in different concentrations to optimize the sensing performance and finding the selectivity.
- Investigate the simulation of the device for understanding the exact physics behind the sensing mechanism occurring in it.
- Investigate the selectivity of the device using soft computing techniques.